



Deep electrical resistivity structure of the northwestern U.S. derived from 3-D inversion of USArray magnetotelluric data



Naser M. Meqbel^{a,b,*}, Gary D. Egbert^a, Philip E. Wannamaker^c, Anna Kelbert^a, Adam Schultz^a

^a CEOAS-Oregon State University, Corvallis, OR, USA

^b Research Centre for Geosciences-Potsdam (GFZ), Potsdam, Germany

^c Energy & Geoscience Institute, University of Utah, Salt Lake City, UT, USA

ARTICLE INFO

Article history:

Accepted 20 December 2013

Available online 22 January 2014

Editor: P. Shearer

Keywords:

USArray
magnetotellurics
electrical resistivity
Pacific NW
tectonics

ABSTRACT

Long period (10–20,000 s) magnetotelluric (MT) data are being acquired across the continental USA on a quasi-regular grid of ~70 km spacing as an electromagnetic component of the National Science Foundation EarthScope/USArray Program. These data are sensitive to fluids, melts, and other orogenic indicators, and thus provide a valuable complement to other components of EarthScope. We present and interpret results of 3-D MT data inversion from 325 sites acquired from 2006–2011 to provide a regional scale view of electrical resistivity from the middle crust to nearly the mantle transition zone, covering an area from NW Washington to NW Colorado. Beneath the active extensional subprovinces in the south-central region, on average we see a resistive upper crust, and then extensive areas of low resistivity in the lower crust and uppermost mantle. Further below, much of the upper half of the upper mantle appears moderately resistive, then subsequently the lower upper mantle becomes moderately conductive. This column suggests a dynamic process of moderately hydrated and fertile deeper upper mantle upwelling during extension, intersection of that material with the damp solidus causing dehydration and melting, and upward exodus of generated mafic melts to pond and exsolve saline fluids near Moho levels. Lithosphere here is very thin. To the east and northeast, thick sections of resistive lithosphere are imaged under the Wyoming and Medicine Hat Cratons. These are punctuated with numerous electrically conductive sutures presumably containing graphitic or sulfide-bearing meta-sediments deeply underthrust and emplaced during ancient collisions. Below Cascadia, the subducting Juan de Fuca and Gorda lithosphere appears highly resistive. Suspected oceanic lithosphere relicts in the central NW part of the model domain also are resistive, including the accreted “Siletzia” terrane beneath the Coast Ranges and Columbia Embayment, and the seismically fast “slab curtain” beneath eastern Idaho interpreted by others as stranded Farallon plate. Upwelling of deep fluid or melt in the Cascade volcanic arc region manifests as conductive features at several scales. These include quasi-horizontal conductive patches under the arc and fore-arc, likely denoting fluids evolved via breakdown of hydrous minerals in the current down-going slab. In the backarc, low resistivities concentrate in “plumes” connecting into a deeper asthenospheric layer to the east, consistent with subduction-driven upwelling of hot, hydrated or melted, asthenospheric mantle. Low resistivities (<10 Ω m) deep beneath the stable cratons suggest higher levels of hydration there, and/or influence of poorly resolved structures outside the array.

© 2013 Elsevier B.V. All rights reserved.

1. Introduction

The northwestern United States exhibits a broad range of tectonic elements with global relevance. Early events include Proterozoic cratonic assembly and rifting to establish the western Laurentian passive margin (Dickinson, 2006; Whitmeyer and Karlstrom, 2007), and then protracted Phanerozoic sedimentation and micro-continental accretion along the paleo-Pacific margin (Wells

et al., 1984; DeCelles, 2004; Wright and Wyld, 2006; Dickinson, 2006, 2008). Subsequently the region has seen extensive bursts of magmatism (Christiansen and Yeats, 1992; Madsen et al., 2006; Humphreys, 2009), interactions with a possible deep mantle plume (Hadley et al., 1976; Geist and Richards, 1993; Smith et al., 2009), large-scale gravitationally-driven extension (Sonder and Jones, 1999; Humphreys and Coblenz, 2007; Dickinson, 2006, 2011), and more localized lithospheric delamination and small-scale convection (e.g., Hales et al., 2005; Darold and Humphreys, 2013). Many of these processes are ongoing such as subduction, arc magmatism, and back-arc extension in Cascadia,

* Corresponding author.

and widespread extension and recent magmatism in the northern Basin and Range (NBR), High Lava Plains (HLP), Yellowstone (YS) and Snake River Plain (SRP) provinces.

High quality, spatially uniform seismic data from the EarthScope transportable array (TA) have led to substantially refined views of complex structure (e.g., Roth et al., 2008; Tian et al., 2009; Eagar et al., 2011; Schmandt and Humphreys, 2010; Obrebski et al., 2011) and anisotropy (Long et al., 2009; Lin et al., 2010; Moschetti et al., 2010) throughout the western U.S. These data have also shed light on regional tectonic history, from recent (Eocene) continental accretion (e.g., Schmandt and Humphreys, 2011), to the fate of the subducting Farallon and Juan de Fuca plates (Sigloch et al., 2008; Sigloch, 2011), to possible subduction/hot spot interactions relevant to patterns of Yellowstone (e.g., Xue and Allen, 2010; James et al., 2011) and High Lava Plains volcanism (Long et al., 2012). Collectively these, and a host of other studies with the seismic TA data, have increased our overall understanding of present and past geodynamic processes, and the physical state of the crust and upper mantle, in terms of temperature, melting, and rheology.

Long period magnetotelluric Transportable Array (MT TA) data are also being collected as part of the EarthScope/USArray program on a similar 70-km grid. These MT data map large-scale spatial variations in bulk electrical resistivity to provide a powerful complement to seismic and other geophysical data. Here we present results from three-dimensional (3-D) inversion of EarthScope long-period MT data from 325 sites acquired in 2006–2011 in a rectangular area from NW Washington to NW Colorado (Fig. 1) to map resistivity from the middle crust to the mantle transition zone.

Electrical resistivity is strongly affected by small amounts of interconnected fluid or melt, which in turn can be controlled by or redefine continental rheology, and are key in element transport, ore deposition and geothermal activity. In some instances, resistivity also reflects presence of graphite or sulphides, often enhanced by metamorphism and fluid remobilization. These can create long-lived conductive signatures such as along early terrane boundaries (Camfield and Gough, 1977; Jones et al., 2005) that otherwise are often cryptic to the surface due to later events. In the upper mantle, in addition to fluids and melts, conductivity can become sensitive to temperature and hydrogen content of the solid state minerals (e.g., Wang et al., 2006; Yoshino, 2010; Poe et al., 2010; Du Frane and Tyburczy, 2012), and may help to define the lithosphere-aesthenosphere boundary (Eaton et al., 2009) or to serve as a proxy for lithospheric refractoriness or refertilization (Wannamaker, 2005; Selway, 2013). All these phenomena are extant in the large-scale resistivity model presented here, which complements previously published seismic results by illuminating 3-D variations of upper mantle and deep crustal hydration, the dynamics of melting from source to residence, and the disposition of fossil, large-scale terrane boundaries.

2. Magnetotelluric data and three dimensional modeling

Reviews of the MT method are provided in Vozoff (1991), Simpson and Bahr (2005) and Chave and Jones (2012). The EarthScope MT data were acquired using conventional long period MT instruments based on fluxgate magnetometers. The recorded time series were processed using a standard robust remote reference approach (e.g., Egbert and Booker, 1986; Egbert, 1997) to estimate the MT impedance (\mathbf{Z}) and the vertical magnetic transfer functions (VTFs). These cover the period range 10–20,000 s with good to high data quality. Although site spacing is very broad (~70 km), distinct regional structures are clear even in simple maps of the MT data (see the supplemental material (SM) for a comprehensive presentation of the data). Broadly speaking, the data show good coherence over groups of stations in diagnostic period ranges

across large areas, reflecting the regional subsurface conductivity distribution revealed in the 3D model subject of this study.

For 3-D modeling and inversion we used the ModEM code of Egbert and Kelbert (2012) parallelized using the scheme of Meqbel (2009). The 3-D model presented in this study is obtained by inverting all components of \mathbf{Z} and VTFs for the 325 stations of Fig. 1. While the full range of period is used for the \mathbf{Z} data, for VTFs we omitted long periods (>6500 s) to avoid external source bias, which becomes important at shorter periods for VTFs than for impedances (e.g., Dmitriev and Berdichevsky, 1979; Egbert, 1989).

Details of our inversion strategy are discussed in the SM. Here we note that i) we assigned error floors of 5% of $|Z_{xy}Z_{yx}|^{1/2}$ for all \mathbf{Z} components and a constant value of 0.03 for VTFs, ii) we used a nested modeling approach to reduce the size of the model domain, iii) we count on a fine enough parameterization in the uppermost part of the model to allow for any near-surface (static shift) effects. We conducted more than 20 inversion runs to assess sensitivity of results to inversion parameters (e.g., grid resolution, model smoothing length scales), or to subsets of data (e.g., \mathbf{Z} or VTFs by themselves, see Fig. S3). In addition, we performed sensitivity studies to verify depth resolution of the data (see Fig. S4). Two main conclusions are worth mentioning here. First, increasing the nominal grid resolution from 25 km to 12.5 km resulted in significantly better data fits. Second, based on the depth resolution study we conclude that structure is resolvable through the upper mantle to ~400 km depth. In the remainder of this paper we focus on a single preferred solution, computed on a 12.5 km resolution grid, and fitting the full dataset to a normalized root mean square misfit of 1.46.

3. The 3D resistivity model and discussion

3.1. Overview

The 3-D resistivity model, which we present in a series of section and plan views, reveals regional to “semi-continental” structures from the middle to lower crust through the upper mantle, with scales of a few hundred to nearly a thousand km. These structures generally reflect the transition from the tectonically active margin in the west, to the more stable North American craton in the east. Many near-surface features of scale comparable to site separation exist as well of course. These serve to represent the effects of shallow local structures (static distortion; e.g., Chave and Jones, 2012; Jones, 2012), but in detail are poorly resolved by the wide site spacing.

To introduce the model, we plot a representative east–west cross section located along latitude 42.5° N in Fig. 2. The principal resistive features in this model cross-section include the oceanic lithosphere beneath the subducting Gorda plate, the deep root of the Wyoming Craton (WYC), and generally resistive middle crust. A very prominent layer of variable but low resistivity (3–50 Ω m) is found near the Moho (white dashed line in Fig. 2), extending from beneath the Klamath Mountains near the coast, through the Cascade volcanic arc (CVA), the NBR and the SRP. This layer generally lies within the lower crust, except below the SRP where the conductivity is especially pronounced and extends into the uppermost mantle, consistent with the results of Kelbert et al. (2012). Some isolated deep crustal conductors also lie within the WYC. In the mantle between the Gorda plate and the WYC, resistivities are moderately low (15–20 Ω m) below ~200 km, but are somewhat higher (~100 Ω m) from ~60 through 150 km. The lowest deep upper mantle resistivities are seen at the far eastern edge of the profile. As we shall discuss, the mantle resistivities are consistent with a thin thermal continental lithosphere only 50–70 km thick

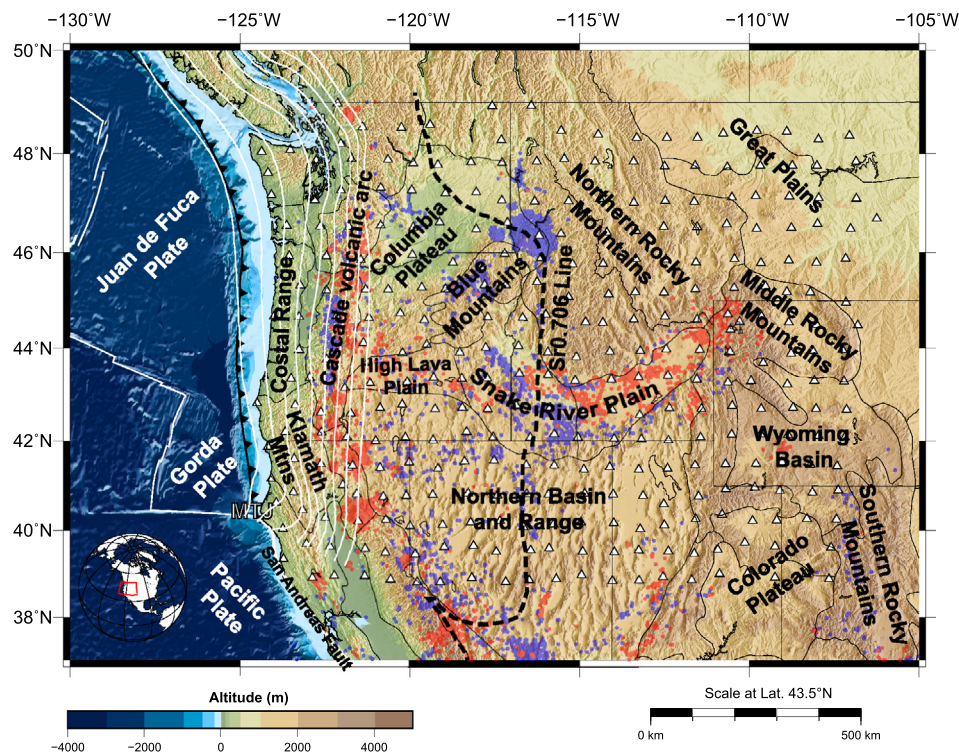


Fig. 1. Map of study area, showing topography, MT site locations (white triangles), physiographic provinces, and key elements of the tectonic setting, including tectonic plates, contours of the subducting slabs (McCroly et al., 2012), the Sr0.706 line (inferred to define the boundary between Precambrian North American and accreted terranes to the west; DeCelles, 2004), and locations of volcanic and intrusive rocks from the NAVDAT database (<http://www.navadat.org>) plotted as blue (age from 17 to 5 Myr) and red (from 5 Myr to present) circles.

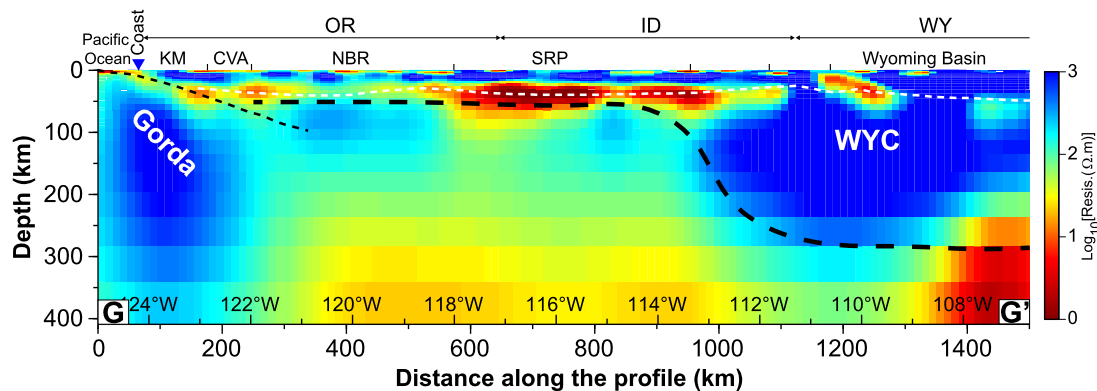


Fig. 2. Representative east-west cross section (latitude 42.5° N, line G–G' in Fig. 3a), illustrating some of the main features in the preferred model. Here, and in other vertical sections, the black short-dashed line denotes the top of the subducting plate (McCroly et al., 2012), and the dashed white line gives an estimate of continental Moho location derived from receiver functions (A. Levander, personal communication; see Levander and Miller, 2012). The heavy black long-dashed line represents a schematic LAB. OR: Oregon; ID: Idaho; WY: Wyoming; KM: Klamath Mountains; CVA: Cascade Volcanic Arc; NBR: Northern Basin and Range; SRP: Snake River Plain; WYC: Wyoming Craton.

in the active provinces of the west, increasing to 200–250 km under the cratonic stable areas.

While the section view captures many important characteristics of the resistivity model, there are also strong variations from north to south, as we show through a series of plan views. For the shallowest layers which span the upper crust, model resolution is poor, due both to lack of short period data (e.g., a skin depth in 100 $\Omega\cdot\text{m}$ at 10 s period is ~ 15 km) and wide site spacing. Nonetheless, even very shallow layers (Fig. 3a) show strong correlation of model character with physiographic province. For example, there are consistently low resistivities on the continental shelf off the west coast (accounting for sediments not included in the prior model), and in the thick sedimentary sections of the Great Plains, while resistivities are consistently high in the Northern Rocky Mountains (NRM), and in the northern Sierra Nevada mountains in California. At

somewhat greater depths (Fig. 3b), the dominantly resistive middle crust is prominent, with local conductive features associated with the CVA and perhaps localized metasedimentary bodies with graphite and sulphides in the eastern Precambrian domains discussed later. There are also mid-crustal conductors in northwestern Utah and western Nevada associated with the highly extended Bonneville and Lahontan basins, and in south-central Washington associated with Tertiary sediments that underlie the Columbia River Basalts (Stanley et al., 1996).

From the lower crust downward the resolving power of the MT TA array and the implications of resistivity for tectonic processes come into their own. We proceed next to describe and interpret the primary resolved structural elements using available constraints on deep temperatures and compositions from tectonic models, seismology and petrology. Our discussion generally

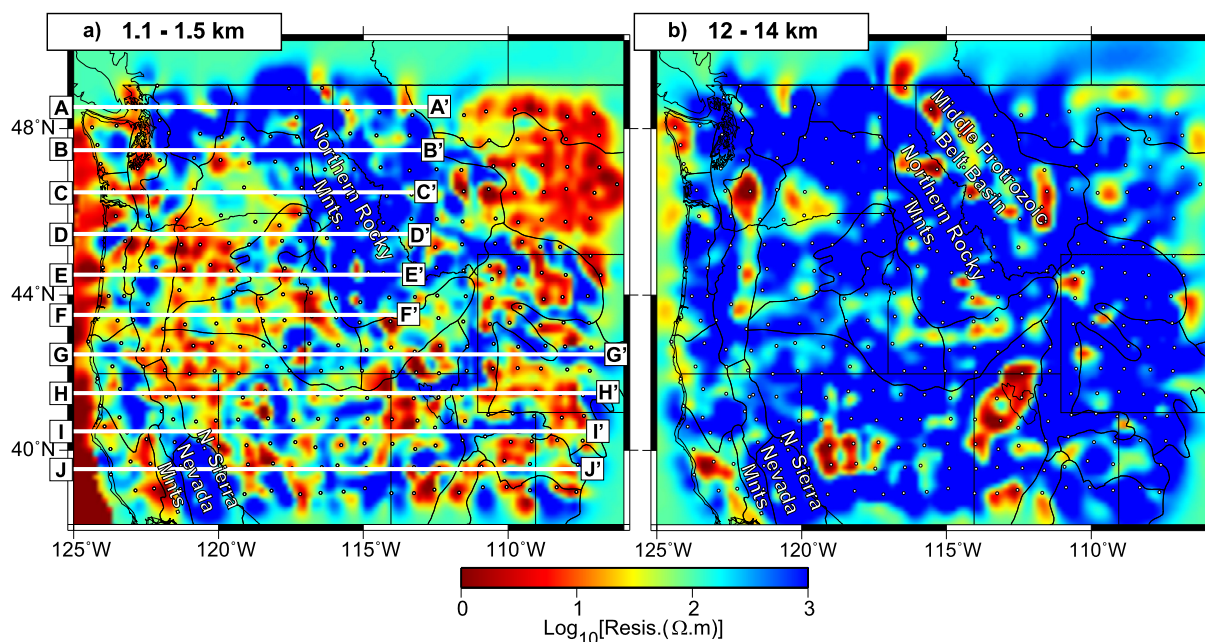


Fig. 3. Resistivity for representative shallow (1.5 km) and mid-crustal (12–14 km) layers. Here, and in other depth sections, site locations are plotted as small dots. White lines in a) give locations of vertical cross-sections presented in Figs. 2, 5 and 8.

proceeds from shallower (lower crustal) to deeper (aesthenospheric) levels, with intermediate sections focused on sub-regions, including the cratonic core, Cascadia subduction zone, the accreted oceanic terrane Siletzia, and the Yellowstone hotspot. The imaged resistivity variations reflect thermo-tectonic processes in subduction, mineralogical hydration/dehydration, magma generation and movement, magma storage and fluid exsolution, stable platform integrity, and the inherited fabric of terrane suturing.

3.2. Conductive lower crust/uppermost mantle

The lateral extent of the conductive layer near the Moho (Fig. 2) is shown in Figs. 4a and 4b, where we plot resistivity for depths of 31–37 km and 54–65 km. Low resistivities are found at these deep crustal/uppermost mantle depths over most tectonically active areas in the region, including the NBR, SRP, and HLP. The conductive lower crust beneath southeastern Oregon is terminated abruptly by the Klamath–Blue Mountain Lineament (KBL; Riddihough et al., 1986), with higher resistivities to the NW beneath the Columbia River Plateau (CRP), and in the Washington and Oregon Coast Ranges (Patro and Egbert, 2008). This more resistive area to the northwest in turn is broken by a north–south band of low resistivity underlying the CVA.

High conductivities in the lower crust in the tectonically active western U.S. have been reported previously (e.g., Stanley et al., 1977, 1990; Wannamaker et al., 1997a, 1997b, 2008; Patro and Egbert, 2008; Kelbert et al., 2012). As discussed in Wannamaker et al. (2008), elevated lower crustal conductivities in extensional areas such as the NBR are most plausibly explained by underplated, hybridized magmas and highly saline fluids exsolved therefrom, residing below the brittle-ductile transition down through Moho depths. Volumes of only a few tenths of percent for hypersaline fluids, to perhaps a few percent for water-undersaturated melts, would be sufficient to match model conductivities (Wannamaker et al., 2008). Figs. 4 and 5 show compellingly how pervasive these lower crustal conductors are in the region. Dense MT profiling including higher frequencies in the NBR has followed fluid connections from such underplating through conductive crustal-scale

fault zones to geothermal systems near-surface (Wannamaker et al., 2008).

In many places the conductive layer appears to extend into the uppermost mantle (Fig. 4b). This is particularly evident beneath the SRP, where Kelbert et al. (2012) inferred that much of the high conductivity must be sub-Moho (Fig. 5). Indeed, surface wave tomography reveals extremely low shear wave velocities in the upper mantle below the SRP, but normal to slightly fast velocities in the lower crust (Gao et al., 2011), relative to regional averages. These higher conductivities in the mantle should reflect presence of melt given likely temperatures, again in quantities of only a few volume percent (e.g., Park et al., 1996; Wannamaker et al., 2008; Kelbert et al., 2012).

High conductivities beneath the Cascade arc and forearc (Figs. 3b, 4a and 5) are interpreted as due to aqueous fluids, in this case associated with slab dehydration and arc magmatism (Wannamaker et al., 1989; Peacock, 2003), although melt could also be present beneath the arc (e.g., Hill et al., 2009). Note that low resistivities beneath the arc generally extend to shallow depths (~10 km or less), much as in the EMSLAB models of Wannamaker et al. (1989) and Evans et al. (2014) for the arc region across north-western Oregon.

3.3. Conductivity anisotropy in the uppermost mantle?

Low resistivities beneath actively extensional areas at Moho and uppermost mantle depths generally have a very “streaky” appearance, with elongate zones of higher and lower resistivity separated by a distance comparable to the TA site spacing (Fig. 4). In the HLP and NBR of southeast Oregon, structures align east–west, swing to a more southwesterly direction in northern Nevada, are north–south further east in the NBR, and lie east–northeast along the magmatic eastern SRP. These conductive and resistive bands may not be well resolved individually, but instead collectively serve to represent bulk electrical anisotropy (with current flowing more readily along the conductive axes) within the otherwise isotropic ModEM model (Heise and Pous, 2001; Wannamaker, 2005). For example, impedance phases for the two source polarizations (corresponding to E–W and N–S current flow) exhibit smooth and

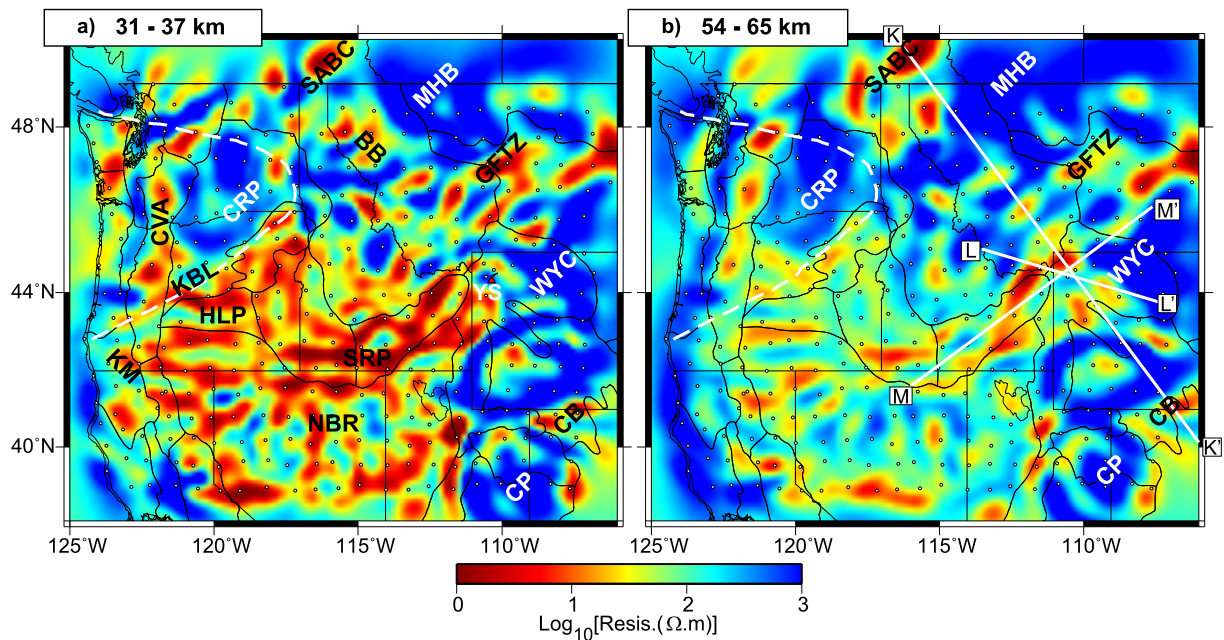


Fig. 4. Model resistivity for layers at a) 31–37 km and b) 54–65 km depth, with features discussed in text labeled. White dashed line represents the outline of Siletzia as defined by Humphreys (2009; see also Gao et al., 2011). White solid lines show profiles for vertical cross-sections of Fig. 6.

consistent differences across southeastern Oregon when sampled at the data sites at a period of 100 s (see SM, Figs. S1a and S1b). With more closely spaced stations one might observe the banding to exhibit finer-scale spacing laterally than seen in the present model.

The east–west orientation of reduced resistivity in the uppermost mantle below southeastern Oregon correlates with the fast-axes for seismic waves inferred from large SKS split times (2.5 s or more) observed in this area (Long et al., 2009). This correlation holds more broadly throughout the NBR and SRP (West et al., 2009; Lin et al., 2010; Figs. 4a and 4b). Seismic anisotropy often is interpreted to result from lattice-preferred orientation (LPO) of olivine (e.g., Karato et al., 2008). However, LPO appears insufficient to explain the resistivity anisotropy for possible crystal water contents at these pressures, and the overall values of resistivity are simply too low for solid state mechanisms at likely Moho-level temperatures (1000–1200 °C; Lachenbruch and Sass, 1978; Yoshino et al., 2006; Poe et al., 2010; Du Frane and Tyburczy, 2012). We thus favor melt as an explanation for the low resistivities in the uppermost mantle (e.g., Yoshino et al., 2010), with shape-preferred orientation of melt pockets or sheets again aligning with mantle shear flow (Zimmerman et al., 1999; Holtzman et al., 2003; Kohlstedt and Holtzman, 2009) possibly accounting for the apparent anisotropy. Indeed, Long et al. (2009) conclude that the unusually large SKS splits observed in southeastern Oregon may require at least a component of anisotropy due to orientation of melt pockets.

3.4. Resistive cratons, conductive sutures

Low resistivities are also found in the 31–65 km depth range (Figs. 4a and 4b) in a northeast trending band within the Great Falls Tectonic Zone (GFTZ), the Belt Basin (BB), on the edges of array coverage to the southeast in the Cheyenne Belt (CB), and to the north in the southern Alberta–British Columbia conductor (SABC; Gough, 1986). Crustal conductive anomalies in these areas are not likely to be associated with present-day fluids or melts, given the Proterozoic age of these geologic features. High conductivities such as these have been frequently observed along

terrane boundaries and sutures, and are most often interpreted as resulting from graphite or sulfides emplaced, metamorphosed and remobilized in the lower crust or deeper during subduction and/or orogenesis (Boerner et al., 1996; Jones et al., 2005; Wannamaker, 2005).

The trends separate major deep resistive blocks in the northeast (Figs. 4a and 4b). The two clearest are readily identified with stable Archean continental lithosphere of the WYC and the Medicine Hat Block (MHB), accreted to the North American core at ~1.8 Ga across the GFTZ (Whitmeyer and Karlstrom, 2007; Gaschnig et al., 2013). The western edge of the MHB is poorly defined, possibly extending into eastern Washington (e.g., Whitmeyer and Karlstrom, 2007), or perhaps truncated at the eastern edge of the Mesoproterozoic Belt Basin in Montana (e.g., Link et al., 1993; Foster et al., 2006). A third substantial resistive mantle feature seen in Figs. 4a and 4b is the Colorado Plateau (CP) in the southeastern corner of the array, to the south of the WYC, of which only the northern part has data coverage. However, the WYC is clearly separated from the moderately resistive southern RM to the southeast by the northeast-trending Cheyenne Belt.

The GFTZ has corresponding gravity and magnetic anomalies and has impressed structural control on essentially the entire Phanerozoic sedimentary cover (Thomas et al., 1987; Boerner et al., 1998). The GFTZ appears to be truncated on the east by the Proterozoic Trans-Hudson Orogen (THO), and so predates amalgamation of the Superior and Hearn provinces (e.g., Whitmeyer and Karlstrom, 2007). Low resistivities in the GFTZ are found over a broad swath (~150–200 km), with northeast trending streaks again suggesting equivalent bulk anisotropy. The conductivity we see in the GFTZ is much stronger than was sampled earlier in southwestern Saskatchewan (cf. Boerner et al., 1998), supporting an interpretation as a locus of accretional collision rather than simply an ancient intra-continental shear zone.

The Cheyenne Belt conductor lies in the northeast striking shear zone which records collision of a large Proterozoic arc terrane with the WYC (Whitmeyer and Karlstrom, 2007) along the eastern edge of our array near the Wyoming–Colorado border (Figs. 4a, 4b and 6a). The Cheyenne Belt may be the southwestern terminus of the continental-scale North American Central Plains (NACP)

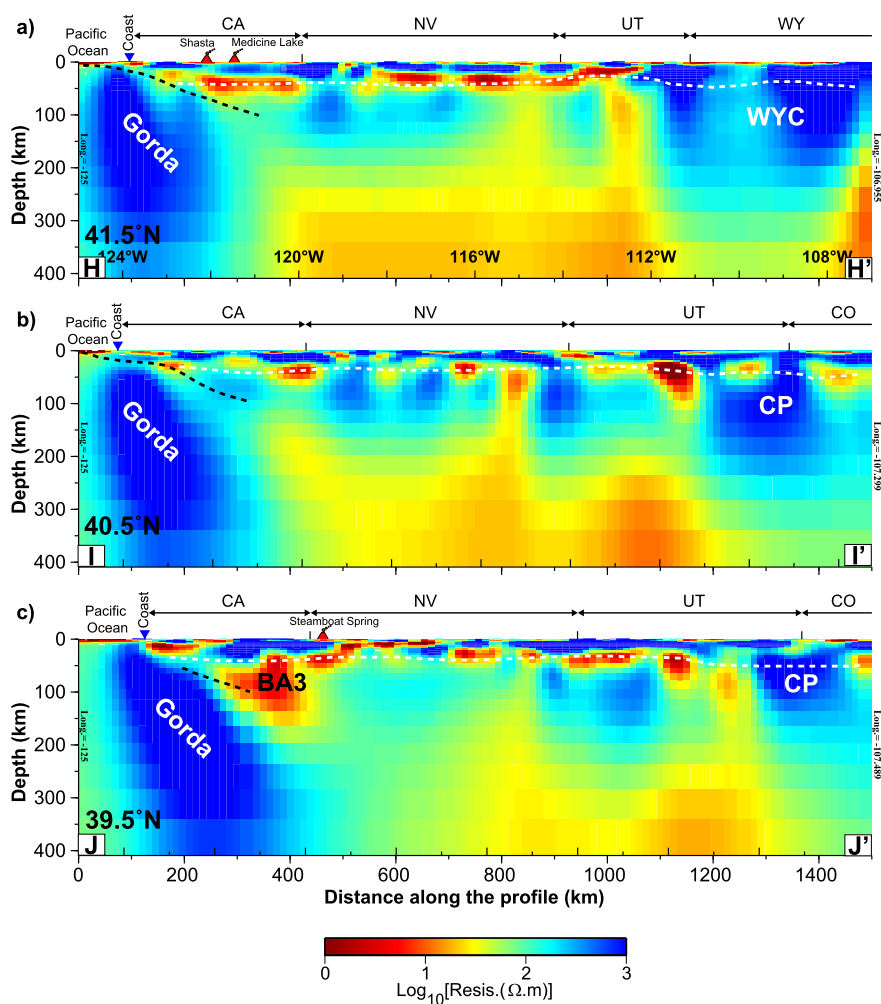


Fig. 5. Resistivity cross sections through the NBR toward the southern end of the array (see Fig. 3a for locations), with top of slab and Moho marked as in Fig. 2. Note N–S continuity of steep upper mantle conductive structures toward the eastern NBR.

anomaly (Alabi et al., 1975; Boerner et al., 1996; Jones et al., 2005; Jones and Savage, 1986), which otherwise lies ~ 200 km beyond the eastern edge of the MT array, and is associated with the THO (Camfield and Gough, 1977). The NACP anomaly, extending from northern Saskatchewan through the Black Hills of South Dakota and into SE Wyoming, is one of the largest known conductive features globally, and may influence other data within our array (see Section 3.6, and SM). Jones et al. (2005) review regional magneto-variational (MV) and MT observations, concluding that high conductivities in the crust are generally well connected along strike but poorly connected across strike, and associated in outcrop with a mix of sheared graphitic metasediments and sulfide mineralization.

The Middle Proterozoic Belt Basin (Link et al., 1993; Lydon, 2007) lies in northwestern Montana, northern Idaho and northeastern Washington, and formed in response to block faulting and subsidence prior to the Late Proterozoic continental margin formation of western Laurentia. It contains nearly 20 km (original section) of sediments including abundant carbonaceous and sulfide-bearing turbidities causing a string of low resistivity anomalies in the middle and lower crust (Bedrosian et al., 2007; cf. Jones et al., 1997) (Figs. 3b, 4a and 6a). Nearly contemporaneous with deposition was extensive mafic magmatism (Moyie group) which contributed to subsidence, metamorphism and sulfide/graphite remobilization (Lydon, 2007). The basin continues into SW British Columbia, just off our array, where it hosts the world-class Sullivan SEDEX sulfide deposit (Lydon, 2007).

Just across the Canadian border with Idaho, the inversion images high conductivities extending well into the mantle (Figs. 6a and 7a). Plots of tipper (SM) suggest that the imaged conductor continues northeastward outside of our array, perhaps connecting with the extensive SABC conductor mapped with early MV array data (Gough, 1986; Gough et al., 1982, 1989). The nature of the SABC is clarified by Nieuwenhuis et al. (in review), who used 3D inversion of MT array data from this area to map what they name the Loverna conductor in the upper mantle at the southern edge of the Hearne craton's Loverna block. This block abuts and underthrusts the Vulcan Structure of southern Alberta (Eaton et al., 1999) separating the Hearne craton from MHB.

Both the Cheyenne Belt and SABC conductors extend to depths approaching 100 km (Fig. 6a), but considering that these structures lie near the edge of our array this result should be treated cautiously. However, in other settings substantial depth extents have been inferred for suturing structures. Moho-level and uppermost mantle conductors observed below the Southern Appalachians mountain chain (Ogawa et al., 1996; Wannamaker, 2005) have been interpreted as deeply under-thrust graphitic sediments associated with the Grenville and Taconic orogenies. Beneath the Slave and Rae provinces of northwestern Canada, fossil subduction signatures assigned to deeply under-thrust metasediments persist to >100 km (Jones et al., 2003; Türkoglu et al., 2009). Association in some cases with diamondiferous kimberlites (Jones et al., 2005) suggests graphitic material can be carried beyond stability

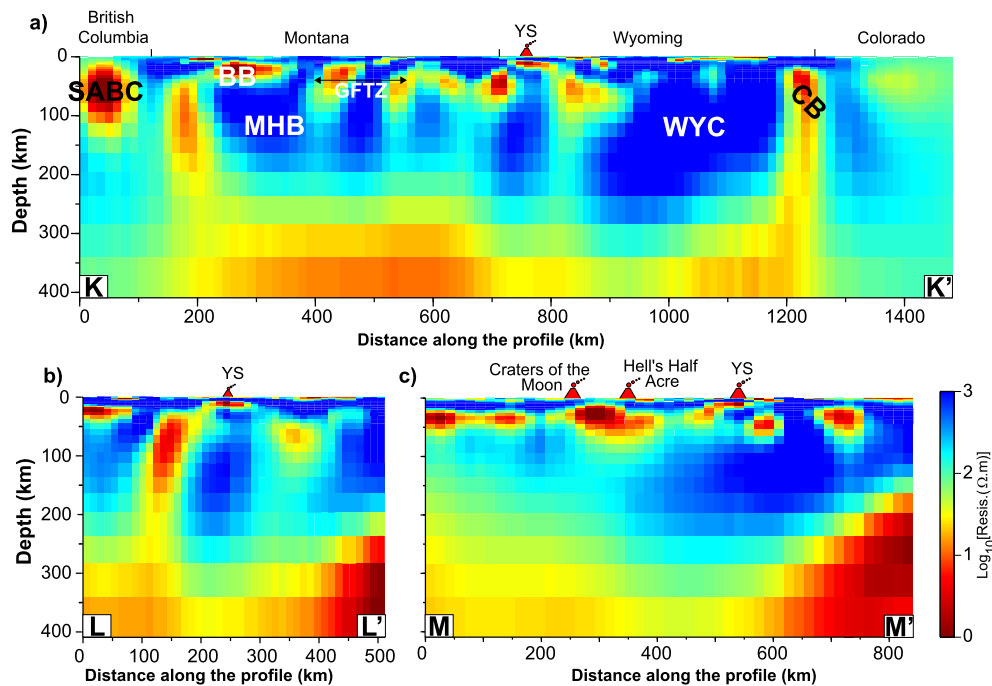


Fig. 6. Cross sections through YS caldera; see Fig. 4b for locations. a) K–K' also transects the principal cratonic features in the eastern part of the model domain, revealing conductive bounding sutures and basins SABC, BB, GFTZ and CB. b) Profile L–L' cuts through the narrow vertical conductive feature NW of YS seen in Figs. 4a and 4b. c) Profile M–M' is aligned with the SRP axis.

to the diamond field (150–160 km depth) where carbon conductivity ceases.

3.5. Siletzia and the slab curtain

In deeper plan views through the upper mantle at 94–113 km, 136–164 km, 197–236 km and 284–341 km depth ranges, a large coherent resistive volume underlies northwestern Washington and northern Idaho (Fig. 7). It dips to the north and east of the resistive CRP lithosphere (Fig. 4), and is coincident with the sub-vertical, high velocity feature (black and white dashed outline in Fig. 7) interpreted by Schmandt and Humphreys (2011) to be a piece of relict subducted Farallon plate, which they refer to as the “slab curtain” (SC). Although directly adjacent to the MHB to the east, the 3D resistivity model suggests that the SC is a separate structure. For example, the section view along latitude 48.5° N (Fig. 8a) shows that the SC is separated from the MHB by a conductive structure extending through the lithosphere, essentially the SW end of the SABC anomaly. Further south along 47.5° N (Fig. 8b), where the two resistive blocks are in contact, there is a step offset in the depth where mantle resistivity increases to 100 Ω m: 300 km for the SC compared to 200 km for the MHB.

Humphreys (2009; see also Gao et al., 2011) interprets the roughly triangular continental block northwest of the Klamath-Blue Mountain Lineament (extending out to the coast, and thus referred to as Siletzia; white dashed outline in Figs. 4a and 4b), as a piece of Farallon lithosphere that accreted within the Columbia Embayment at ~48 Ma (Madsen et al., 2006; Wells and McCaffrey, 2013). In eastern Washington, Siletzia is interpreted to have underthrust older crust. Schmandt and Humphreys (2011) extend this model to explain the SC, interpreting the vertical zone of high seismic velocity as the down-dip (already subducted) continuation of the accreted Farallon plate. In this model, Farallon subduction was flat prior to accretion, associated with Laramide orogeny. After subduction jumped to the west, the slab rolled back, allowing asthenospheric flow into a newly opening mantle wedge, and leading

to an intense surge of Challis magmatic activity as the thoroughly hydrated lithosphere heated up.

The MT results are clearly consistent with this conceptual model. The inferred Siletzia province is almost uniformly resistive, except where broken by the Cascade arc. The lithospheric mantle beneath the CRP is resistive to depths of ~100 km (Figs. 4b and 7a), with the high resistivities extending off the eastern and northern edges, dipping steeply to ~300 km. These high resistivities are expected for oceanic lithosphere, similar to the subducting Juan de Fuca plate (JdF) and Gorda plates (Fig. 2; also see Section 3.6). Indeed, the resistivity section through the putative slab curtain at 48.5° N and 47.5° N looks remarkably like a pair of “en echelon” subduction zones, with the 60 Ma subduction zone ~500 km to the east, just where the fossil arc suggests it should be (e.g., see Fig. 2 in Schmandt and Humphreys, 2011).

3.6. Subduction zone and backarc

Resistive oceanic lithosphere appears as a continuous feature all along the western edge of the continent (plan view of Fig. 7, section view of Fig. 8). The imaged top of this resistive feature generally agrees well with seismic constraints on slab geometry to 90 km depth (McCroory et al., 2012). Resolution tests (see SM) suggest that a conductive oceanic asthenosphere (which would be expected; e.g., Wannamaker et al., 1989; Worzewski et al., 2010) is permitted by the MT TA data, although not required mainly because we have no marine coverage. The land data require only a layer of sufficiently high resistance to constrict ocean induced currents near the surface, with rapid shorting into the mantle once the backarc is reached.

The eastern boundary of the resistive oceanic lithosphere appears to curve around to the east and extend along the southwestern edge of the array. While much of this resistive area is beyond the array coverage, the initial bend to the east near latitude 40° N (Fig. 7) is in fact fairly well sampled, and consistent with tomographic images (Sigloch et al., 2008; Schmandt and Humphreys, 2010; James et al., 2011), which show high P and S

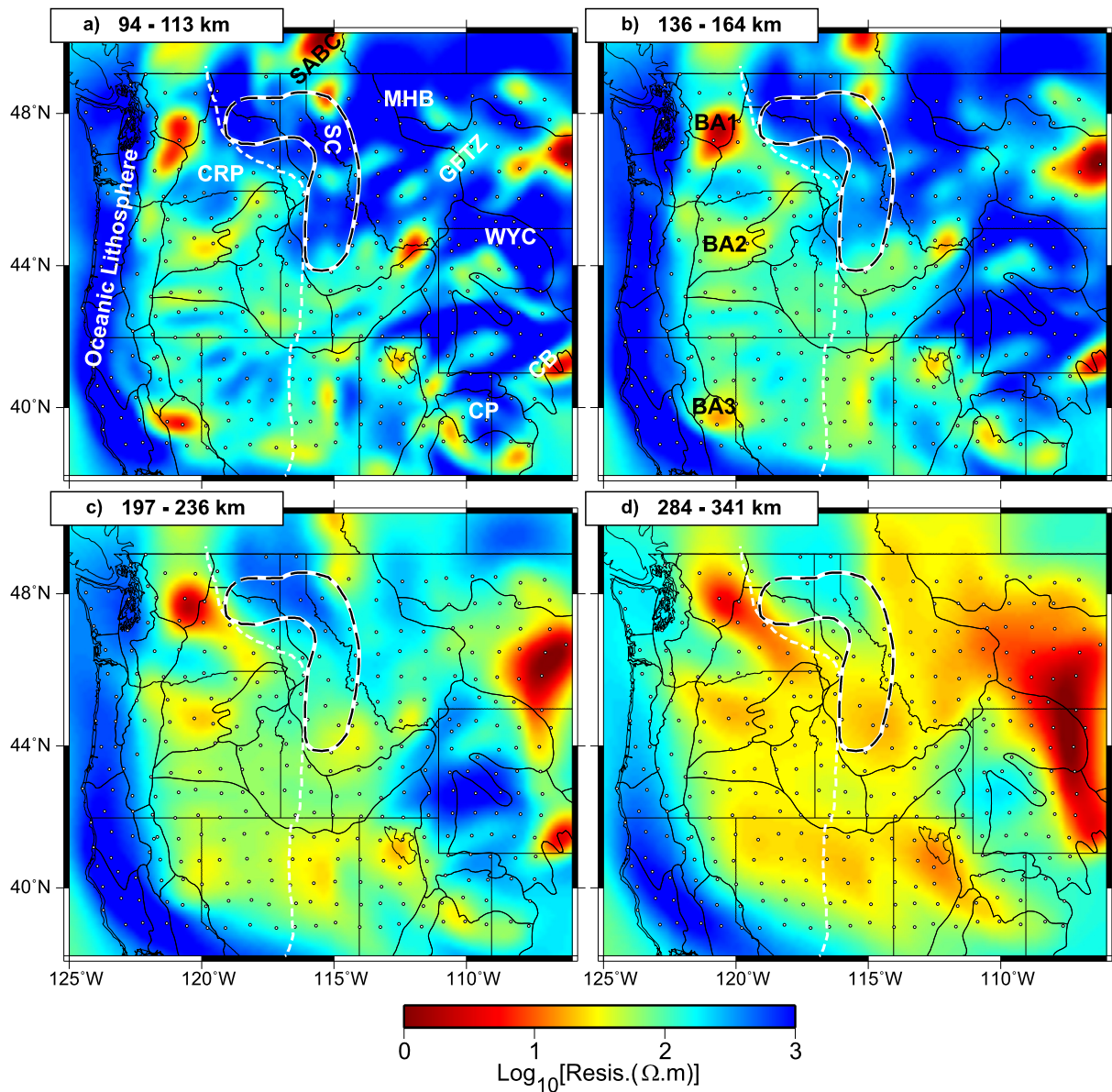


Fig. 7. Model resistivity for layers at 94–113, 136–164, 197–236 and 284–341 km depth, with features discussed in text labeled. Dashed white and black line indicates location of the fast seismic anomaly (SC), interpreted by [Schmandt and Humphreys \(2011\)](#) to be relict Farallon plate. Dashed white line shows the Sr0.706 line, and BA1, BA2 and BA3 are three Back Arc conductive features discussed in the text.

velocities curving eastward at 200–300 km depth at this latitude. Thus, while the eastward sweep of high resistivity may be exaggerated by inversion smoothing and edge effects, the general trend probably reflects the geometry of the subducted plate in this area. We note also that sparse legacy MT data south of our coverage in the Great Valley block of central California show substantial oceanic electrical current trapping within lower resistivity of the upper crust, with high resistivities below to great depth ([Mackie et al., 1988, 1997](#)).

The section views of [Fig. 8](#) commonly show deep-crustal, quasi-horizontal patches of low resistivity in the near fore-arc region of the CVA. We believe these are analogous to the lower crustal zones of accumulated fore-arc fluids interpreted from previous dense MT transect studies in Cascadia and elsewhere ([Wannamaker et al., 1989; Soyer and Unsworth, 2006; Worzewski et al., 2010](#)). The fluids are believed to evolve from breakdown (eclogitization) of greenschist and higher-grade hydrate minerals in the downgoing slab under thermal control ([Peacock, 2003; Worzewski et al., 2010](#)), which buoyantly rise and collect in the deep crust. Given

likely temperatures, these are not considered to be melts, although they may verge on such as the arc is approached. In the dense MT studies (e.g., [Wannamaker et al., 1989; Evans et al., 2014; McGary, 2013](#)), the fore-arc limit of these conductors appears to correspond to loss of coherent seismic contrasts along the top of the subducting plate, as seen in receiver function surveys ([Bostock et al., 2002; Rondenay et al., 2008a, 2008b](#)). The trenchward limit of such conductors may lie close to generation zones of episodic tremor and slip (ETS) which [Audet et al. \(2010\)](#) argue may result from high fluid pressure near the tip of the mantle wedge. Resolution of such details requires more densely sampled broadband MT data on land, and ideally also offshore ([Evans et al., 2002; Worzewski et al., 2010](#)).

The fore-arc low resistivity features commonly extend eastward beneath the arc ([Figs. 2, 4, 5 and 8](#)), although there is significant variability along the subduction zone. Sometimes these features reach the mid-upper crust ([Fig. 3b](#)), where they can be interpreted to stem from shallower level structural disruption, magma emplacement, or fluid egress. Again, such structures have been

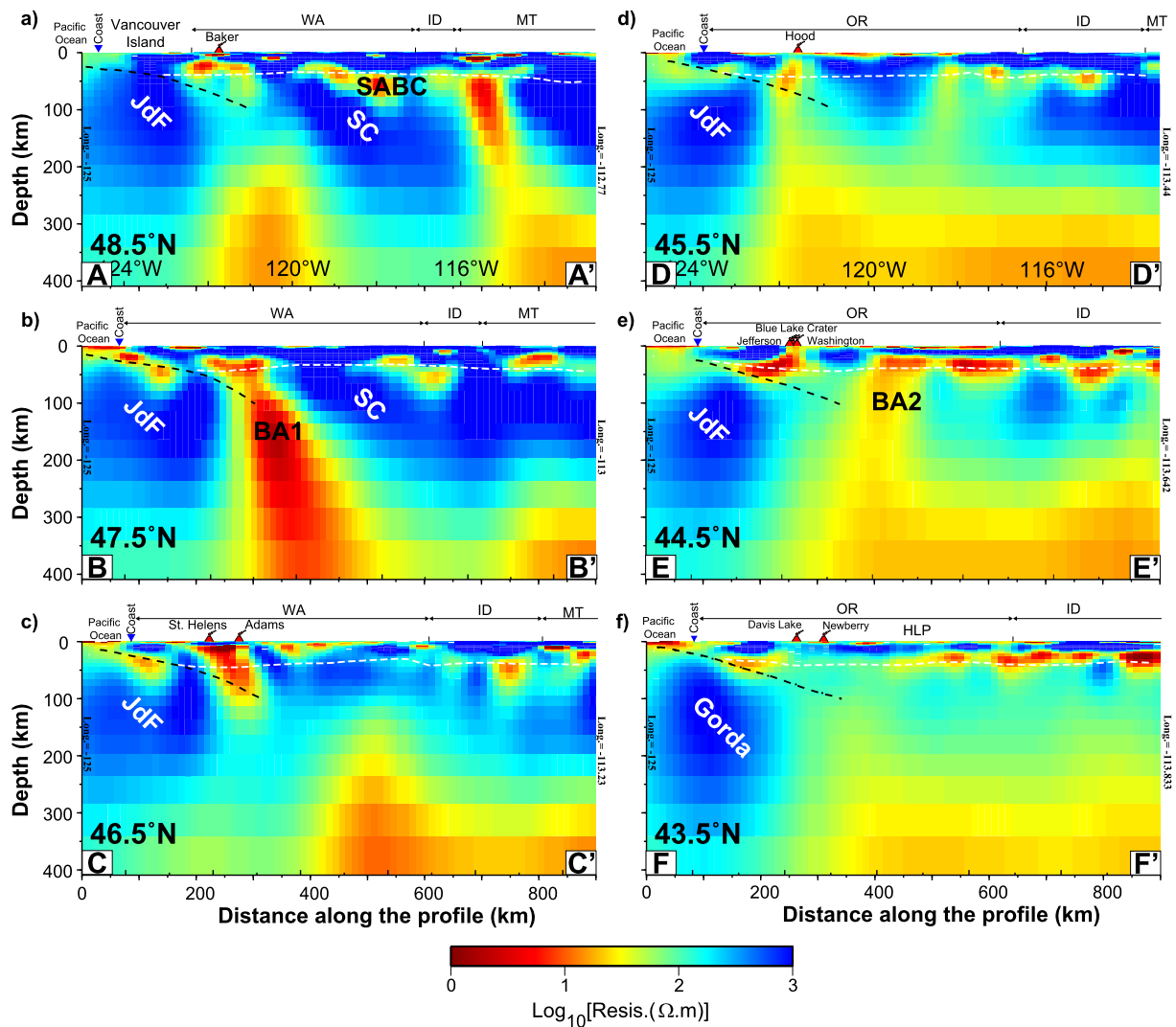


Fig. 8. Vertical sections (see Fig. 3a for locations) through the northern part of the model, crossing the Pacific coast (inverted triangles) and extending into the back arc. Top of subducting plate and Moho are marked as in Fig. 2, and prominent composite volcanoes are projected onto nearby sections for reference.

resolved to much greater detail in finer-spaced MT surveys including shorter period data in Cascadia (Wannamaker et al., 1989; Hill et al., 2009; Evans et al., 2014), and other arc settings (e.g., Ingham et al., 2009; Heise et al., 2010).

Larger-scale zones of low resistivity (10–100 Ω m) rise to shallow depths in the backarc above the subducting plate (Figs. 7b and 8), with “plumes” of low resistivity nearing the sub-arc conductive zone in several places. In particular, three localized conductive features (labeled on Fig. 7b) are worth more detailed discussion. BA1 (in Washington State), is a very conductive structure seen dipping steeply to the east in vertical section B–B’ at 47.5° N (Fig. 8b). At shallow depths this conductor tilts to the south towards the Cascade arc volcanoes Mt Rainier, Mt Saint Helens and Mt Adams, possibly approaching the crustal conductor imaged beneath this area by Hill et al. (2009). At depth, this structure extends below 200 km, where it bends to the southeast (Figs. 7c and 7d). Seismic tomography images high velocities in this area at 200 km depth (e.g., Tian et al., 2009; Schmandt and Humphreys, 2010; James et al., 2011), interpreted as the subducting plate. We suggest that the high conductivities of BA1 may represent upwelling asthenospheric corner flow driven by subduction, and are thus above the seismically fast (and resistive) subducting plate, with the actual interface depth lacking good resolution in the MT model. The bend of BA1 to the southeast sug-

gests that the asthenospheric flow is constrained to a relatively narrow conduit by the highly viscous SC to the east (Figs. 8a and 8b). Given that an appreciable amount of slab water may be carried far inland of an arc (Hacker, 2008), some flux melting of the upper mantle could be promoted within most of this conductive zone.

South of BA1 there is a resistive gap in the backarc in southern Washington. South of the Washington/Oregon border, resistivities fall again; moderately low values (~ 30 Ω m) extend west of the arc in the deepest layers near the Columbia River (Figs. 7c, 7d and 8d) just where seismic tomography images an apparent gap in the high velocities of the JdF plate (Rasmussen and Humphreys, 1988; Schmandt and Humphreys, 2010; James et al., 2011; Chu et al., 2012). Although Roth et al. (2008) suggest that this gap may be an imaging artifact resulting from a strong low velocity anomaly to the east, Sigloch (2011) argues that the gap can be connected to a tear in the slab which extends far to the northeast. Chu et al. (2012) combined tomography and waveform modeling to provide more detailed images of the subducting plate, which they model as extending no deeper than ~ 150 km near the Oregon/Washington border. East of Seattle, Washington, they image a segment of high P-velocity JdF slab that dips southeastward, extending to at least 250 km depth, lying nearly coincident with the resistive zone in southern Washington (Fig. 7d).

Similar interpretation can be applied to conductive upwellings BA2 and BA3, with details of geometry influenced by differences in the subducting plate and relict structures in the continental mantle. BA2 in the central part of the arc in east-central Oregon (Figs. 7b and 8e) is most prominent in section E–E' at 44.5° N, but also is visible in section D–D' at 45.5° N, rising more directly under the arc. It coincides with a prominent slow anomaly seen in seismic tomography images (e.g., Roth et al., 2008; Schmandt and Humphreys, 2010; James et al., 2011; Darold and Humphreys, 2013). Similarly, the southerly conductor BA3 (Fig. 7b; section views I–I' and J–J' in Figs. 5b and 5c) is just east of the south edge of the Gorda Plate in northeastern California. If thermal and deformational effects from slab window formation south of Cape Mendocino (Dickinson and Snyder, 1979) are restricted to a band within ~80 km of the coast, as suggested by Hayes and Furlong (2007) and McCrory et al. (2009), the high conductivities of BA3 should also reflect backarc processes. BA3 may also correlate with a geographically coincident, low V_s anomaly that develops below 100 km depth in the tomographic image of Gilbert et al. (2012).

3.7. Yellowstone

The Yellowstone region represents one of the most intense upper mantle upwelling zones in the western U.S. with massive caldera eruptions in the geologic record (Smith et al., 2009). Resistivity inversions of MT TA data localized to this area have yielded disparate results (Zhdanov et al., 2011; Kelbert et al., 2012). Our model resembles the second of these in showing high conductivity in the uppermost mantle beneath the SRP and in the middle crust below YS, but a moderately resistive (100–300 Ω m) lowermost crust and upper mantle directly beneath the caldera (Fig. 6). We note that both our study and that of Kelbert et al. (2012) inverted all four complex impedance and both complex tipper elements with very good fits throughout the period range.

Seismic surface and body wave tomography models resolve low velocities, attributed to melt, to depths of ~200 km beneath the caldera, extending to the southwest beneath the SRP (Smith et al., 2009; Wagner et al., 2010; Schmandt & Humphreys, 2010; Obrebski et al., 2011; Tian and Zhao, 2012). Near the caldera, body wave models show the low velocity zone dipping to the WNW and weakening between 200–400 km, before strengthening again in the transition zone and lower mantle. The seismic results thus are consistent with some sort of plume of hotter and possibly melting material below YS. One might expect zones of melting to show low resistivity if melt is interconnected over distances that are at least a large fraction of their depth (e.g., Yoshino et al., 2010).

However, the seismic attenuation study of Adams and Humphreys (2010) reveals further complexities, which may help to reconcile the MT and seismic results. These authors found that above ~200–250 km, seismic attenuation beneath the caldera was significantly lower than in the adjacent surrounding mantle. The relatively high surrounding attenuation may represent significant mantle hydration, with reduced attenuation in the hotter plume core explained by melt induced dehydration of the solid matrix. In fact, the incipient low-temperature melting of rising upper mantle plume induced by intracrystalline water should be of very low volume (<0.1%, Adams and Humphreys, 2010) and unlikely to segregate (i.e., develop long range interconnection), consistent with the relatively high resistivities we see. At shallower levels (<100 km) the seismic and EM results could be reconciled if melt in this domain does not possess long range horizontal interconnection, but instead tends to coalesce and leave the system in steep, episodic conduits with little effect on horizontal MT source fields. In fact, the recent laboratory experiments of Garapić et al. (2013) show that grain boundary melt should lead to seismic attenuation, but

the model of Adams and Humphreys shows low attenuation to almost arbitrarily shallow levels in the YS core zone.

Our wider aperture model suggests low resistivities in the mantle off to the WNW side of the modern caldera, where resistivities of 10 Ω m or less extend to 150–200 km depth, and with somewhat weaker lows to the ESE (sections L–L' and M–M' in Fig. 6; also Fig. 4b). Schmandt and Humphreys (2010) show a strong V_p/V_s anomaly closely coincident with the deeply extending low resistivity to the northwest side of the SRP. Typically such seismic anomalies are attributed to low rigidity volumes such as melts, which as noted must possess long range interconnection to reduce resistivity.

3.8. Aesthenospheric mantle conductivity

A definition of the aesthenosphere is the deeper zone of the upper mantle that is ductile and weak, and is disconnected mechanically from the overlying lithosphere which is relatively strong and coherent (e.g., Turcotte and Schubert, 2002). We divide our section view in Fig. 2 into material that belongs to one or the other of these two fundamental domains across the lithosphere–aesthenosphere boundary (LAB) (long dashed black line in Fig. 2). For the active magmatic or extensional regions from the CVA through the HLP and SRP to YS, the relatively shallow LAB is consistent with petrologic evidence for high mantle temperatures ~70 km beneath the SRP (Leeman et al., 2009), and at even shallower depths beneath the HLP (Long et al., 2012; Till et al., 2013). Such an LAB conforms to seismic receiver function estimates as well (Levander and Miller, 2012). Temperature profiles estimated from both P- and S-wave tomography (Goes and van der Lee, 2002) imply almost adiabatic conditions with a potential temperature T_p near 1300 °C from ~70 km down through the upper mantle. Below the cratonic elements to the east, the tomographically inferred adiabat and LAB are not reached until depths ~200 km (Goes and van der Lee, 2002). Constraining the domain and temperature of the aesthenosphere in this way allows us use the inverted electrical resistivity for other purposes, namely, to understand state of hydration and melting there.

Below the active regions in Fig. 2, the upper aesthenosphere from just below the crust to depths of 150–200 km is not conductive, but rather lies near 100 Ω m. This may be a minimal value given that inversion regularization tends to bleed conductive lower crust downward, so higher resistivities in a thin layer of thermal mantle lithosphere cannot be ruled out. From ~200 km downward, resistivities mainly are considerably lower, in the 15–30 Ω m range. Under the cratonic areas, the data do not resolve an upper and a lower zone of aesthenospheric resistivity, but rather exhibit a simple but large drop in resistivity to values of a few 10's of Ω m or even <10 Ω m on the eastern edge of the study area. As we show in the SM, these latter high, deep conductivities may reflect contamination by the NACP, 200 km further east. Basic character of the section in Fig. 2 is borne out in the other sections of Fig. 5.

To facilitate further discussion of deep model resistivity variations we construct spatially averaged conductivity-depth profiles for eight areas (shown in Fig. 9a), each relatively homogeneous below roughly 100 km depth. Four of the areas (solid lines in Fig. 9a) are in tectonically active areas, with the remaining four in the older and more stable part of the continent to the east (dashed lines in Fig. 9a). Areas beneath the subducting JdF oceanic plate are not considered here. The profiles are shown for the two groups in Figs. 9c and 9d, together with laboratory-based estimates of resistivity profiles (Poe et al., 2010), assuming an aesthenospheric T_p of 1300 °C and an adiabatic gradient of 0.3 °C/km (Turcotte and Schubert, 2002).

For all of the tectonically active areas (Fig. 9c) resistivities for depths of ~70–150 km are consistent with lab results for dry

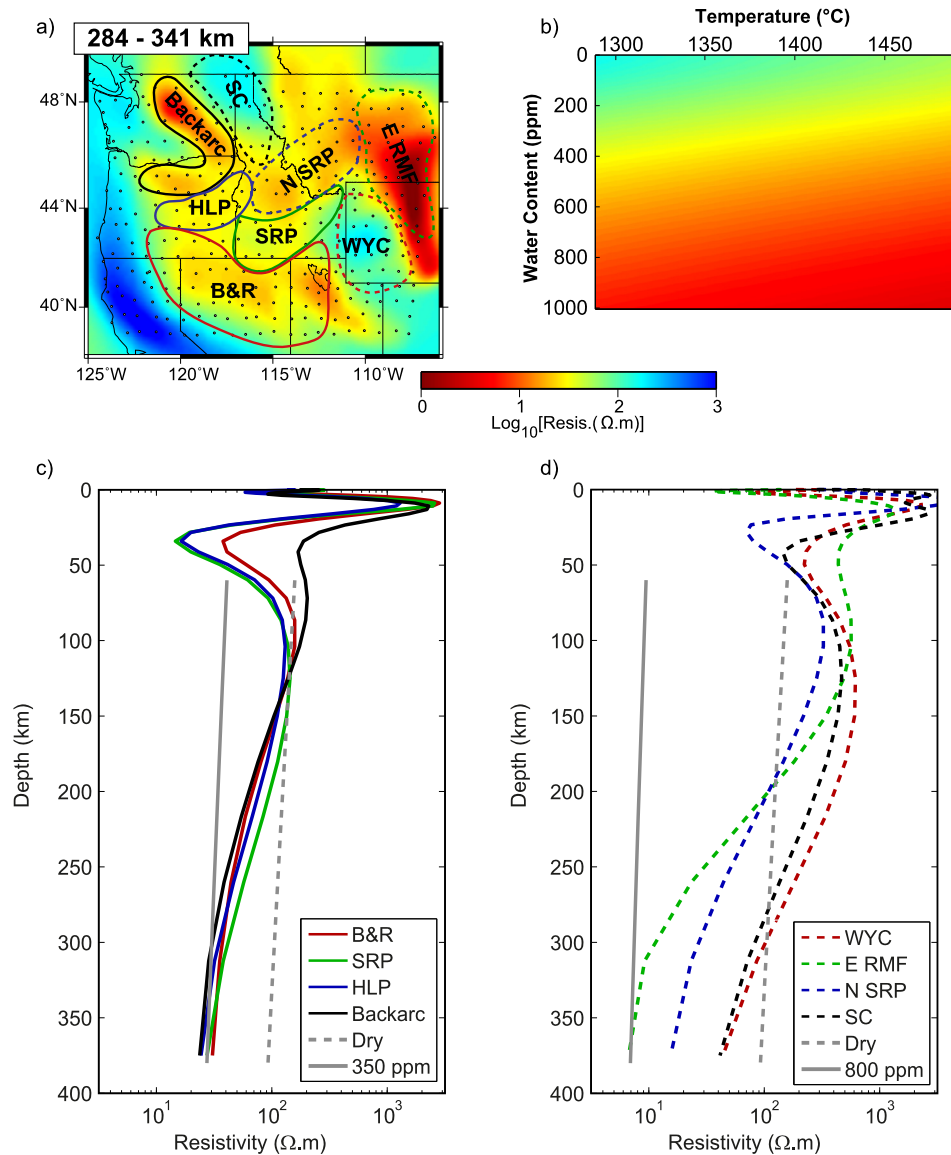


Fig. 9. a) Model resistivity for aesthenospheric layer at 284–341 km, subdivided into patches used to compute spatially averaged conductivity–depth profiles. Isotropic olivine resistivity, computed from the laboratory results of [Poe et al. \(2010\)](#), are plotted as a function of temperature ($^{\circ}\text{C}$) and water content (weight ppm) in b) using the same color scale. Profiles are shown for tectonically active areas in panel c), and for more stable/cratonic areas in d), along with profiles derived from the lab results, assuming a potential temperature of 1300°C , and an adiabatic gradient of $0.3^{\circ}\text{C}/\text{km}$.

olivine within uncertainty, assuming the above temperatures. This suggests that the shallowest aesthenosphere in this area has been purged of volatiles and low-melting components during the region’s extensive Late Cenozoic history of magmatism and is now nearly dry. Much of that melting in the upper mantle is what we interpret to have ponded near Moho depth levels to produce the widespread and pronounced peak in conductivity discussed in Section 3.2 with [Figs. 4a, 4b and 5](#). Of course, a portion of this melting is visible at the surface in the lavas widespread over the region today. All of the averaged resistivity profiles in [Fig. 9c](#) are quite similar below 100 km, and necessitate increasing hydration with depth (~ 350 ppm by 300 km) to match the lab results.

For a plan view perspective, the 284–341 km model layer in [Fig. 9a](#) should be well within the aesthenosphere throughout the model domain (except in the subduction zone). To compare the model slice to laboratory results we also plot ([Fig. 9b](#)) resistivity at 300 km depth for a range of temperatures and water contents, computed from the geometric average of the single crystal laboratory resistivity measurements for olivine given in [Poe](#)

[et al. \(2010\)](#). Over most of the domain, model resistivities at this depth are consistent with the laboratory results for reasonable mantle temperatures, assuming moderate levels of hydration (several hundred ppm). An adiabat alone however is insufficient to explain the shapes of the resistivity profiles in the presumed aesthenosphere. Melting is not required, below 200 km, and in fact should not be occurring at assumed temperatures given the limited inferred water content. The experimentally-based “damp” solidi in [Hirschmann et al. \(2009\)](#) show that a water content of 400–500 ppm and an adiabat similar to ours would induce incipient melting in the depth range 150–200 km, consistent with our interpretation.

For all of the cratonic areas ([Fig. 9d](#)), resistivities compatible with aesthenospheric temperatures are not reached until depths of at least 200 km, with the thickest thermal lithosphere (300 km) found beneath the southeastern part of the Wyoming craton, and in the “slab curtain” beneath eastern Washington and northern Idaho. The lowest deep resistivities are found east of the Rocky Mountain front in Montana and Wyoming. Although this average

may possibly be contaminated by the NACP to the east, a large patch of the low resistivity (10 Ω m) extending over much of eastern Montana is well within the array coverage and is considered well resolved. The area north of the SRP is also somewhat more conductive (15–20 Ω m) at depths below 300 km. This area has been imaged as an area of low V_s at somewhat greater depth (~400 km) by James et al. (2011) (see also Sigloch et al., 2008, and Tian et al., 2009), who have interpreted this anomaly as a gap or tear in the JdF plate through which hot lower mantle (plume) material might rise to the YS–SRP area (James et al., 2011; Sigloch, 2011).

4. Comparison to Bedrosian and Feucht model

Bedrosian and Feucht (2014; hereinafter BF2013) also present a 3D resistivity model for the NW U.S., based on inversion of a subset of the MT TA data used in our study. They used the code of Siripunvaraporn et al. (2005) to invert impedances (but not VTFs) from 241 sites (roughly those west of the Wyoming–Idaho border), in 10 logarithmically spaced period bands from 10–10,000 s (compared to the full, denser set of 22 bands extending up to 20,000 s, used here). Details of the numerical grid (slightly coarser in BF2013), boundary treatment, and model regularization are also somewhat different. The nRMS data misfit for the BF2013 model is 3.1 compared to the nRMS of 1.46 achieved here, both assuming error floors of 5%. Difference in fit appears largest at the longest and (to a lesser extent) shortest periods (BF2013; also personal communication, P. Bedrosian). Principal model features nonetheless are generally similar between the two studies. In particular, both models show resistive oceanic lithosphere, similar patterns of Moho-level high conductivity throughout the active west, and thick resistive cratons to the east and northeast with evidence for deep fossil conductive structures such as the GFTZ and Belt Basin.

We believe our tighter fit and wider site aperture permit structure to depths of 400 km, allowing us to make important inferences about mantle hydration and melting; models with little or no structure at these depths can be obtained if data fit is relaxed sufficiently (Fig. S4 and related discussion). Consequently, our high model conductivities in the back arc (also seen in BF2013) appear connected to deeper layers of elevated asthenospheric conductivity, suggestive of upwelling. At shallower depths, the high crustal conductivities beneath and often afore the CVA are more pronounced in our model. In the uppermost mantle our model more clearly exhibits elongate streaking, which we have suggested may represent finer scale anisotropy. These smaller-scale features developed in our models as the inversion converged to tighter data fits; lesser fitting models from earlier inversion stages were smoother.

In the CRP, we image resistive lithosphere comparable to Coast Range basement and fit the data there quite well. This supports the interpretation of Humphreys (2009) and Schmandt and Humphreys (2011) that the lithospheric block from the coast to near the Idaho border is all Siletzia, accreted to North America at ~48 Ma and overprinted by modern arc volcanism. The BF2013 model CRP resistivities are lower, suggesting to its authors that Siletzia is terminated on the east near the modern arc and that the CRP lithosphere is much older. BF2013 interpret the deep resistive block beneath eastern Washington and Idaho (similar in both models, but imaged to greater depth in ours) as Archean craton. Model interpretation here must be informed by many constraints (see Schmandt and Humphreys, 2011, and BF2013) and warrants more thought. The most significant difference between the two models is in south central Washington, where we image a conductive feature (interpreted as a sedimentary basin beneath the basalt cover) restricted to upper-mid crustal depths, while in BF2013 this feature appears to extend through the crust. Depth resolution and

character of fitting of the MT data remain issues deserving close attention.

5. Summary and conclusions

The vast majority of previous MT campaigns have acquired data in one, or a few, dense linear profiles, quite different from the layout used for the EarthScope MT array discussed here. With widely spaced sites distributed on a quasi-uniform grid covering a large area, tried-and-true interpretation approaches developed for profiles are generally inapplicable, and the very sparse distribution of sites raises concerns about effects of near-surface static distortion, and aliasing due to under-sampling. Indeed, in the planning stages of EarthScope questions were raised about whether the proposed widely-spaced array sampling strategy would prove useful for imaging Earth resistivity. The 3D inversion results presented here, and previously (Patro and Egbert, 2008; Kelbert et al., 2012; Zhdanov et al., 2012), largely lay this concern to rest. While there is still much to learn about 3D inversion of MT array data, and while issues of under-sampling and near-surface distortion still deserve attention (e.g., as suggested by differences with the BF2013 results), it seems clear that quite useful images of large scale regional variations in Earth resistivity can be obtained with the EarthScope sampling strategy. Although many fine-scale details are of course poorly resolved, the broad MT TA array coverage provides for the first time a coherent 3D view of regional-scale crustal and upper mantle resistivity variations in the northwestern U.S. The quasi-uniform site distribution is well suited to 3D inversion, and the wide aperture of the array, and high quality of long period data, allow resolution of lateral variations of resistivity nearly to the transition zone.

In broadest terms, the 3D resistivity model reflects the transition from the tectonically active margin in the west, to more stable North American tectonic craton in the east. Throughout much of the west, resistivities are very low in the lower crust and uppermost mantle, almost certainly due to melt and magmatic fluids. Such conductive features have been commonly observed in previous MT surveys in this region, but our regional scale images nonetheless provide new perspectives, clearly outlining the geographic distribution, and demonstrating just how pervasive these lower crustal conductors are. Our results also suggest a possible component of anisotropy in the mantle associated with melt alignment, and reveal regional differences—e.g., low resistivities appear to extend more deeply into the mantle beneath the SRP than in the adjacent NBR.

The 3D model also confirms another common observation from prior MT surveys across the globe, namely that high conductivities are often found in ancient suture zones, bounding resistive cratonic blocks. Our model again provides new perspectives, delineating, at least at large scale, the geometry of these cratonic blocks and sutures in the northwestern USA in three dimensions. More broadly, 3D inversion of widely spaced MT array data clearly has great potential for reconnaissance mapping of relict continental structural boundaries.

Our 3D images of the Cascadia subduction zone and backarc provide highly complementary views to the 2D interpretations of dense MT profiles from this area and greatly expand the context. Qualitatively, similar first order features are observed, with low resistivities in the near forearc likely due to slab dehydration and fluid accumulation in the crust. Though broader-scale, our 3D inversion of the widely spaced MT TA data captures the main features, and gives some hints of how these vary all along the arc. The 3D images further suggest connections to deeper structures in the backarc, where we image generally low resistivities. The variability of back-arc resistivities along the subduction zone is consistent with physiographic, geochemical and seismic evidence for arc

segmentation (Guffanti and Weaver, 1988; Schmidt et al., 2008; Porritt et al., 2011). The overall large-scale pattern is consistent with subduction driven upwelling of hot, probably hydrated, and possibly melting asthenospheric mantle to a small number of localized “plumes”. Some of the variations in upflow may reflect control by more impenetrable upper mantle structures, e.g., subducted oceanic lithosphere.

Mantle resistivities east of the backarc are consistent with a thermal continental lithosphere that is only 50–70 km thick in the active provinces of the west, increasing to 200–250 km under the eastern cratonic areas. Constraining upper mantle temperatures beneath the active regions to be an adiabat, the profile of asthenospheric resistivities implies that the lower half of the upper mantle is relatively hydrated and fertile (e.g., by Farallon subduction; Humphreys, 2009), whereas the upper half appears dehydrated and refractory from melting. The formed melts are those whose products are imaged today at Moho levels above where they hybridize and release fluids. These conclusions on mantle hydration derive directly from constraints on temperature, and highlight the value of such independent information in reducing non-uniqueness in physico-chemical interpretations from resistivity.

While a detailed inter-comparison is beyond the scope of this paper, we note that our MT model is broadly consistent with recent EarthScope seismic TA images of the area. For example, surface wave studies reveal low shear wave velocities in many of the lower crustal and upper mantle areas which we image as conductive, the resistive cratons are seismically fast, and the seismically fast CRP lithosphere and slab curtain are highly resistive. There are of course areas of anti-correlation (e.g., the Washington backarc, where low resistivities are co-located with fast velocities at 200 km depth), which may in part relate to the resolving capability for conductors relative to resistors in MT. But there are also important areas where the MT provides new insights about structures and processes. These include upper mantle melt source depletion and dehydration, widespread Moho level magma accumulation and evolution, the loci of fluids liberated in subduction, and the locations and compositional implications of major terrane sutures and relict basins. Clearly, more focused efforts on joint interpretation of these seismic and MT datasets are warranted.

Finally, this study underscores the need for a large array aperture to image deep structure. Several large deep features near the edges of the model are enigmatic, and may indicate boundary effects. These include the excessive thickness of resistive oceanic lithosphere, with no evidence for an underlying conductive asthenosphere, high resistivities at depth along the southeastern edge of the array in northern California and Nevada, and high conductivities at the east edge of our array toward the THO. These model features may be artifacts resulting from a combination of poorly sampled large-scale structure near the array edge, and incorrect (and poorly known) model boundary conditions.

Acknowledgements

G.D. Egbert, N.M. Meqbel and A. Kelbert were supported by NSF grant EAR1053628, and DOE grant DE-FG02-06ER15819. P.E. Wannamaker was funded by NSF grant EAR08-43725 under the EarthScope program. A. Schultz was supported by Incorporated Research Institutions for Seismology (IRIS) subcontract 75-MT, under National Science Foundation Cooperative Agreement No. EAR-0733069. Data from the TA network are made freely available as part of the EarthScope USArray facility (<http://www.earthscope.org>), operated by Incorporated Research Institutions for Seismology (IRIS) and supported by the National Science Foundation, under Cooperative Agreements EAR-0323309, EAR-0323311, EAR-0733069. The main inversion results were accomplished using computation resources of the GFZ German Research Centre

for Geosciences, Potsdam. The authors are grateful to the editors and the two anonymous reviewers for their comments and suggestions which helped to improve clarity of the manuscript. We thank numerous districts of the U.S. Forest Service and Bureau of Land Management, Yellowstone and Grand Teton National Parks, the collected State land offices, and the many private landowners who permitted access to acquire the MT TA data.

Appendix A. Supplementary material

Supplementary material related to this article can be found online at <http://dx.doi.org/10.1016/j.epsl.2013.12.026>.

References

- Adams, D.C., Humphreys, E.D., 2010. New constraints on the properties of the Yellowstone mantle plume from P and S wave attenuation tomography. *J. Geophys. Res.* 115, B12311.
- Alabi, A., Camfield, P., Gough, D., 1975. The North American central plains conductivity anomaly. *Geophys. J. R. Astron. Soc.* 43, 815–833.
- Audet, P., Bostock, M.G., Boyarko, D.C., Brudzinski, M.R., Allen, R.M., 2010. Slab morphology in the Cascadia fore arc and its relation to episodic tremor and slip. *J. Geophys. Res.* 115, B00A16.
- Bedrosian, P.A., Feucht, D.W., 2014. Structure and tectonics of the northwestern United States from EarthScope USArray magnetotelluric data. *Earth Planet. Sci. Lett.* 402, 275–289. <http://dx.doi.org/10.1016/j.epsl.2013.07.035> (in this volume).
- Bedrosian, P.A., Stephen, E., Pellerin, L., 2007. Structure and tectonic evolution of the Belt Basin, Montana/Idaho from geophysical constraints. *Geol. Soc. Am. Abstr. Progr.* 39 (6), 492.
- Boerner, D., Kurtz, R., Craven, J., 1996. Electrical conductivity and Paleo-Proterozoic foredeeps. *J. Geophys. Res.* 101, 13775–13791.
- Boerner, D., Craven, J., Kurtz, R., Ross, G., Jones, F., 1998. The Great Falls Tectonic Zone: suture or intracontinental shear zone?. *Can. J. Earth Sci.* 35, 175–183.
- Bostock, M., Hyndman, R., Rondenay, S., Peacock, S., 2002. An inverted continental Moho and serpentinization of the forearc mantle. *Nature* 417, 536–538.
- Camfield, P., Gough, D., 1977. A possible Proterozoic plate boundary in North America. *Can. J. Earth Sci.* 14, 1229–1238.
- Chave, A.D., Jones, A.G. (Eds.), 2012. *The Magnetotelluric Method: Theory and Practice*. Cambridge Univ. Press, 552 pp.
- Christiansen, R.L., Yeats, R.S., 1992. Post-Laramide geology of the US Cordilleran region. In: Burchfiel, B.C., Lipman, P.W., Zoback, M.L. (Eds.), *The Cordilleran Orogen: Contemporaneous U.S.* In: *Geol. North. Am.*, vol. G-3. Geological Society of America, pp. 261–406.
- Chu, R., Schmandt, B., Helmberger, D.V., 2012. Juan de Fuca subduction zone from a mixture of tomography and waveform modeling. *J. Geophys. Res.* 117, B03304.
- Darold, A., Humphreys, E., 2013. Upper mantle seismic structure beneath the Pacific Northwest: A plume-triggered delamination origin for the Columbia River flood basalt eruptions. *Earth Planet. Sci. Lett.* 365, 232–242.
- DeCelles, P., 2004. Late Jurassic to Eocene evolution of the Cordilleran thrust belt and foreland basin system, western USA. *Am. J. Sci.* 304, 105–168.
- Dickinson, W.R., 2006. Geotectonic evolution of the Great Basin. *Geosphere* 2, 353–368.
- Dickinson, W.R., 2008. Accretionary Mesozoic–Cenozoic expansion of the Cordilleran continental margin in California and adjacent Oregon. *Geosphere* 4, 329–353.
- Dickinson, W.R., 2011. The place of the Great Basin in the Cordilleran orogen. In: Steinginger, R., Pennell, B. (Eds.), *Great Basin Evolution and Metallogeny, 2010 Symposium*. Geological Society of Nevada, Nevada, pp. 419–436.
- Dickinson, W.R., Snyder, W.S., 1979. Geometry of triple junctions related to San Andreas transform. *J. Geophys. Res.* 84, 561–572.
- Dmitriev, V.I., Berdichevsky, M.N., 1979. The fundamental model of magnetotelluric sounding. *Proc. IEEE* 67, 1033–1044.
- Du Frane, W.L., Tyburczy, J.A., 2012. Deuterium-hydrogen exchange in olivine: Implications for point defects and electrical conductivity. *Geochem. Geophys. Geosyst.* 13, Q03004.
- Eagar, K.C., Fouch, M.J., James, D.E., Carlson, R.W., 2011. Crustal structure beneath the High Lava Plains of eastern Oregon and surrounding regions from receiver function analysis. *J. Geophys. Res.* 116, B02311.
- Eaton, D.W., Ross, G.M., Clowes, R.M., 1999. Seismic-reflection and potential-field studies of the Vulcan structure, western Canada: A Paleoproterozoic Pyrenees?. *J. Geophys. Res.* 104, 23255–23269.
- Eaton, D.W., Darbyshire, F., Evans, R.L., Grütter, H., Jones, A.G., Yuan, X., 2009. The elusive lithosphere–asthenosphere boundary (LAB) beneath cratons. *Lithos* 109, 1–22.
- Egbert, G.D., 1989. Multivariate analysis of geomagnetic array data II: Random source models. *J. Geophys. Res.* 94, 14249–14265.
- Egbert, G.D., 1997. Robust multiple-station magnetotelluric data processing. *Geophys. J. Int.* 130, 475–496.

- Egbert, G.D., Booker, J.R., 1986. Robust estimation of geomagnetic transfer functions. *Geophys. J. R. Astron. Soc.* 87, 173–194.
- Egbert, G.D., Kelbert, A., 2012. Computational recipes for electromagnetic inverse problems. *Geophys. J. Int.* 189, 251–267.
- Evans, R.L., Chave, A.D., Booker, J.R., 2002. On the importance of offshore data for magnetotelluric studies of ocean–continent subduction systems. *Geophys. Res. Lett.* 29, 1302.
- Evans, R.L., Wannamaker, P.E., McGary, R.S., Eisenbeck, J., 2014. Electrical structure of the central Cascadia subduction zone: the EMSLAB Lincoln Line revisited. *Earth Planet. Sci. Lett.* 402, 265–274. <http://dx.doi.org/10.1016/j.epsl.2013.04.021> (in this volume).
- Foster, D.A., Mueller, P.A., Mogk, D.W., Wooden, J.L., Vogl, J.J., 2006. Proterozoic evolution of the western margin of the Wyoming craton: Implications for the tectonic and magmatic evolution of the northern Rocky Mountains. *Can. J. Earth Sci.* 43, 1601–1619.
- Gao, H., Humphreys, E.D., Yao, H., van der Hilst, R.D., 2011. Crust and lithosphere structure of the northwestern US with ambient noise tomography: Terrane accretion and Cascade arc development. *Earth Planet. Sci. Lett.* 304, 202–211.
- Garapic, G., Faul, U., Brisson, E., 2013. High-resolution imaging of the melt distribution in partially molten upper mantle rocks: evidence for wetted two-grain boundaries. *Geochem. Geophys. Geosyst.*
- Gaschnig, R.M., Vervoort, J.D., Lewis, R.S., Tikoff, B., 2013. Probing for Proterozoic and Archean crust in the northern US Cordillera with inherited zircon from the Idaho batholith. *Geol. Soc. Am. Bull.* 125, 73–88.
- Geist, D., Richards, M., 1993. Origin of the Columbia Plateau and Snake River plain: Deflection of the Yellowstone plume. *Geology* 21, 789–792.
- Gilbert, H., Yang, Y., Forsyth, D., Jones, C., Owens, T., Zandt, G., Stachnik, J., 2012. Imaging lithospheric foundering in the structure of the Sierra Nevada. *Geosphere* 8, 1310–1330.
- Goes, S., van der Lee, S., 2002. Thermal structure of the North American uppermost mantle inferred from seismic tomography. *J. Geophys. Res.* 107, 2050.
- Gough, D.I., 1986. Mantle upflow tectonics in the Canadian Cordillera. *J. Geophys. Res.* 91, 1909–1919.
- Gough, D.I., Bingham, D.K., Ingham, M.R., Alabi, A., 1982. Conductive structures in southwestern Canada: a regional magnetometer array study. *Can. J. Earth Sci.* 19 (8), 1680–1690.
- Gough, D.I., McKirdy, D.M., Woods, D.V., Geiger, H., 1989. Conductive structures and tectonics beneath the EMSLAB land array. *J. Geophys. Res.* 94 (B10), 14099–14110.
- Guffanti, M., Weaver, C.S., 1988. Distribution of late Cenozoic volcanic vents in the Cascade Range: Volcanic arc segmentation and regional tectonic considerations. *J. Geophys. Res.* 93, 6513–6529.
- Hacker, B.R., 2008. H₂O subduction beyond arcs. *Geochem. Geophys. Geosyst.* 9, Q03001.
- Hadley, D.M., Stewart, G.S., Ebel, J.E., 1976. Yellowstone: seismic evidence for a chemical mantle plume. *Science* 193, 1237–1239.
- Hales, T.C., Abt, D., Humphreys, E., Roering, J.J., 2005. A lithospheric instability origin for Columbia River flood basalts and Wallowa Mountains uplift in northeast Oregon. *Nature* 438, 842–845.
- Hayes, G.P., Furlong, K.P., 2007. Abrupt changes in crustal structure beneath the Coast Ranges of northern California – developing new techniques in receiver function analysis. *Geophys. J. Int.* 170, 313–336.
- Heise, W., Pous, J., 2001. Effects of anisotropy on the two-dimensional inversion procedure. *Geophys. J. Int.* 147, 610–621.
- Heise, W., Caldwell, T.G., Bibby, H.M., Bennie, S.L., 2010. Three-dimensional electrical resistivity image of magma beneath an active continental rift, Taupo Volcanic Zone, New Zealand. *Geophys. Res. Lett.* 37, L10301.
- Hill, G.J., Caldwell, T.G., Heise, W., Chertkoff, D.G., Bibby, H.M., Burgess, M.K., Cull, J.P., Cas, R.A., 2009. Distribution of melt beneath Mount St Helens and Mount Adams inferred from magnetotelluric data. *Nat. Geosci.* 2, 785–789.
- Hirschmann, M.M., Tenner, T., Aubaud, C., Withers, A., 2009. Dehydration melting of nominally anhydrous mantle: The primacy of partitioning. *Phys. Earth Planet. Inter.* 176, 54–68.
- Holtzman, B., Kohlstedt, D., Zimmerman, M., Heidelbach, F., Hiraga, T., Hustoft, J., 2003. Melt segregation and strain partitioning: implications for seismic anisotropy and mantle flow. *Science* 301, 1227–1230.
- Humphreys, E., 2009. Relation of flat subduction to magmatism and deformation in the western United States. In: *Backbone of the Americas: Shallow Subduction, Plateau Uplift, and Ridge and Terrane Collision*, p. 85.
- Humphreys, E.D., Coblenz, D.D., 2007. North American dynamics and western US tectonics. *Rev. Geophys.* 45, RG3001.
- Ingham, M., Bibby, H., Heise, W., Jones, K., Cairns, P., Dravitzki, S., Bennie, S., Caldwell, T., Ogawa, Y., 2009. A magnetotelluric study of Mount Ruapehu volcano, New Zealand. *Geophys. J. Int.* 179, 887–904.
- James, D.E., Fouch, M.J., Carlson, R.W., Roth, J.B., 2011. Slab fragmentation, edge flow and the origin of the Yellowstone hotspot track. *Earth Planet. Sci. Lett.* 311, 124–135.
- Jones, A., 2012. Distortion of magnetotelluric data: Its identification and removal. In: *The Magnetotelluric Method: Theory and Practice*, pp. 219–302.
- Jones, A.G., Savage, P.J., 1986. North American Central Plains conductivity anomaly goes east. *Geophys. Res. Lett.* 13, 685–688.
- Jones, A.G., Katsube, T.J., Schwann, P., 1997. The longest conductivity anomaly in the world explained: sulphides in fold hinges causing very high electrical anisotropy. *J. Geomagn. Geoelectr.* 49, 1619–1629.
- Jones, A.G., Lezaeta, P., Ferguson, I.J., Chave, A.D., Evans, R.L., Garcia, X., Spratt, J., 2003. The electrical structure of the Slave craton. *Lithos* 71, 505–527.
- Jones, A.G., Ledo, J., Ferguson, I.J., 2005. Electromagnetic images of the Trans-Hudson orogen: the North American Central Plains anomaly revealed. *Can. J. Earth Sci.* 42, 457–478.
- Karato, S., Jung, H., Katayama, I., Skemer, P., 2008. Geodynamic significance of seismic anisotropy of the upper mantle: new insights from laboratory studies. *Annu. Rev. Earth Planet. Sci.* 36, 59–95.
- Kelbert, A., Egbert, G.D., deGroot Hedlin, C., 2012. Crust and upper mantle electrical conductivity beneath the Yellowstone Hotspot Track. *Geology* 40, 447–450.
- Kohlstedt, D.L., Holtzman, B.K., 2009. Shearing melt out of the Earth: An experimentalist's perspective on the influence of deformation on melt extraction. *Annu. Rev. Earth Planet. Sci.* 37, 561–593.
- Lachenbruch, A.H., Sass, J.H., 1978. Models of an extending lithosphere and heat flow in the Basin and Range province. In: Smith, R.B., Eaton, G.P. (Eds.), *Cenozoic Tectonic and Regional Geophysics of the Western Cordillera*. In: *Geol. Soc. Am. Mem.*, vol. 152, pp. 209–250.
- Leeman, W.P., Schutt, D.L., Hughes, S.S., 2009. Thermal structure beneath the Snake River Plain: Implications for the Yellowstone hotspot. *J. Volcanol. Geotherm. Res.* 188, 57–67.
- Levander, A., Miller, M.S., 2012. Evolutionary aspects of lithosphere discontinuity structure in the western US. *Geochem. Geophys. Geosyst.* 13, Q0AK07.
- Lin, F.-C., Ritzwoller, M.H., Yang, Y., Moschetti, M.P., Fouch, M.J., 2010. Complex and variable crustal and uppermost mantle seismic anisotropy in the western United States. *Nat. Geosci.* 4, 55–61.
- Link, P., Christie-Blick, N., Devlin, W., Elston, D., Horodyski, R., Levy, M., Miller, J., Pearson, R., Prave, A., Stewart, J., et al., 1993. Middle and Late Proterozoic stratified rocks of the western US Cordillera, Colorado Plateau, and Basin and Range province. In: Reed, J.C., Bickford, M.E., et al. (Eds.), *Precambrian: Coterminous U.S.* In: *Geol. North Am.*, vol. 2. Geological Society of America, Boulder, pp. 463–596.
- Long, M.D., Gao, H., Klaus, A., Wagner, L.S., Fouch, M.J., James, D.E., Humphreys, E., 2009. Shear wave splitting and the pattern of mantle flow beneath eastern Oregon. *Earth Planet. Sci. Lett.* 288, 359–369.
- Long, M.D., Till, C.B., Druken, K.A., Carlson, R.W., Wagner, L.S., Fouch, M.J., James, D.E., Grove, T.L., Schmerr, N., Kincaid, C., 2012. Mantle dynamics beneath the Pacific Northwest and the generation of voluminous back-arc volcanism. *Geochem. Geophys. Geosyst.* 13, Q0AN01.
- Lydon, J.W., 2007. Geology and metallogeny of the Belt–Purcell Basin. In: *Mineral Deposits of Canada: A Synthesis of Major Deposit-Types, District Metallogeny, the Evolution of Geological Provinces, and Exploration Methods*. In: *Miner. Depos. Div., Spec. Publ.*, vol. 5. Geological Association of Canada, pp. 581–607.
- Mackie, R., Bennett, B., Madden, T., 1988. Long-period magnetotelluric measurements near the central California coast: A land-locked view of the conductivity structure under the Pacific Ocean. *Geophys. J. Int.* 95, 181–194.
- Mackie, R.L., Livelybrooks, D.W., Madden, T.R., Larsen, J.C., 1997. A magnetotelluric investigation of the San Andreas fault at Carrizo Plain, California. *Geophys. Res. Lett.* 24, 1847–1850.
- Madsen, J., Thorkelson, D., Friedman, R.M., Marshall, D., 2006. Cenozoic to Recent plate configurations in the Pacific Basin: Ridge subduction and slab window magmatism in western North America. *Geosphere* 2, 11–34.
- McCrory, P.A., Wilson, D.S., Stanley, R.G., 2009. Continuing evolution of the Pacific–Juan de Fuca–North America slab window system—A trench–ridge–transform example from the Pacific Rim. *Tectonophysics* 464, 30–42.
- McCrory, P.A., Blair, J.L., Waldhauser, F., Oppenheimer, D.H., 2012. Juan de Fuca slab geometry and its relation to Wadati–Benioff zone seismicity. *J. Geophys. Res.* 117, B09306.
- McGary, R.S., 2013. The CAFE experiment: a joint seismic and MT investigation of the Cascadia subduction system. Ph.D. thesis. Massachusetts Institute of Technology and Woods Hole Oceanographic Institution.
- Meqbel, N.M.M., 2009. The electrical conductivity structure of the Dead Sea Basin derived from 2D and 3D inversion of magnetotelluric data. Ph.D. thesis. Free University of Berlin.
- Moschetti, M., Ritzwoller, M., Lin, F., Yang, Y., 2010. Seismic evidence for widespread western-US deep-crustal deformation caused by extension. *Nature* 464, 885–889.
- Nieuwenhuis, G., Unsworth, M., Pana, D., Craven, J., Bertrand, E., in review. Three dimensional resistivity structure of Southern Alberta, Canada: Implications for Pre-Cambrian tectonics. *Geophys. J. Int.*
- Obrebski, M., Allen, R.M., Pollitz, F., Hung, S.-H., 2011. Lithosphere–asthenosphere interaction beneath the western United States from the joint inversion of body-wave traveltimes and surface-wave phase velocities. *Geophys. J. Int.* 185, 1003–1021.
- Ogawa, Y., Jones, A.G., Unsworth, M.J., Booker, J.R., Lu, X., Craven, J., Roberts, B., Parmelee, J., Farquharson, C., 1996. Deep electrical conductivity structures of the Appalachian Orogen in the southeastern US. *Geophys. Res. Lett.* 23, 1597–1600.

- Park, S.K., Hirasuna, B., Jiracek, G.R., Kinn, C., 1996. Magnetotelluric evidence of lithospheric mantle thinning beneath the southern Sierra Nevada. *J. Geophys. Res.* 101, 16241–16255.
- Patro, P.K., Egbert, G.D., 2008. Regional conductivity structure of Cascadia: Preliminary results from 3D inversion of USArray transportable array magnetotelluric data. *Geophys. Res. Lett.* 35, L20311.
- Peacock, S.M., 2003. Thermal structure and metamorphic evolution of subducting slabs. In: Eiler, J. (Ed.), *Inside the Subduction Factory*, vol. 138. AGU American Geophysical Union, pp. 7–22.
- Poe, B.T., Romano, C., Nestola, F., Smyth, J.R., 2010. Electrical conductivity anisotropy of dry and hydrous olivine at 8 GPa. *Phys. Earth Planet. Inter.* 181, 103–111.
- Porritt, R.W., Allen, R.M., Boyarko, D.C., Brudzinski, M.R., 2011. Investigation of Cascadia segmentation with ambient noise tomography. *Earth Planet. Sci. Lett.* 309, 67–76.
- Rasmussen, J., Humphreys, E., 1988. Tomographic image of the Juan de Fuca Plate beneath Washington and western Oregon using teleseismic P-wave travel times. *Geophys. Res. Lett.* 15, 1417–1420.
- Riddihough, R., Finn, C., Couch, R., 1986. Klamath–Blue Mountain lineament, Oregon. *Geology* 14, 528–531.
- Rondenay, S., Abers, G., Creager, K., Malone, S., MacKenzie, L., Zhang, Z., van Keken, P., Wech, A., Sweet, J., Melbourne, T., et al., 2008a. CAFE: a seismic investigation of water percolation in the Cascadia subduction zone. In: *AGU Fall Meeting Abstracts*, vol. 1, p. 08.
- Rondenay, S., Abers, G.A., van Keken, P.E., 2008b. Seismic imaging of subduction zone metamorphism. *Geology* 35, 275–278.
- Roth, J.B., Fouch, M.J., James, D.E., Carlson, R.W., 2008. Three-dimensional seismic velocity structure of the northwestern United States. *Geophys. Res. Lett.* 35.
- Schmandt, B., Humphreys, E., 2010. Complex subduction and small-scale convection revealed by body-wave tomography of the western United States upper mantle. *Earth Planet. Sci. Lett.* 297, 435–445.
- Schmandt, B., Humphreys, E., 2011. Seismically imaged relict slab from the 55 Ma Siletzia accretion to the northwest United States. *Geology* 39, 175–178.
- Schmidt, M.E., Grunder, A.L., Rowe, M.C., 2008. Segmentation of the Cascade Arc as indicated by Sr and Nd isotopic variation among diverse primitive basalts. *Earth Planet. Sci. Lett.* 266, 166–181.
- Selway, K.M., 2013. On the causes of electrical conductivity in stable lithosphere. *Surv. Geophys.* <http://dx.doi.org/10.1007/s10712-013-9235-1>.
- Sigloch, K., 2011. Mantle provinces under North America from multifrequency P wave tomography. *Geochem. Geophys. Geosyst.* 12, Q02W08.
- Sigloch, K., McQuarrie, N., Nolet, G., 2008. Two-stage subduction history under North America inferred from multiple-frequency tomography. *Nat. Geosci.* 1, 458–462.
- Simpson, F., Bahr, K., 2005. *Practical Magnetotellurics*. Cambridge Univ. Press, 254 pp.
- Siripunvaraporn, W., Egbert, G.D., Lenbury, Y., Uyeshima, M., 2005. Three dimensional magnetotelluric inversion: data-space method. *Phys. Earth Planet. Inter.* 150, 3–14.
- Smith, R.B., Jordan, M., Steinberger, B., Puskas, C.M., Farrell, J., Waite, G.P., Husen, S., Chang, W.-L., O'Connell, R., 2009. Geodynamics of the Yellowstone hotspot and mantle plume: Seismic and GPS imaging, kinematics, and mantle flow. *J. Volcanol. Geotherm. Res.* 188, 26–56.
- Sonder, L.J., Jones, C.H., 1999. Western United States extension: How the West was widened. *Annu. Rev. Earth Planet. Sci.* 27, 417–462.
- Soyer, W., Unsworth, M., 2006. Deep electrical structure of the northern Cascadia (British Columbia, Canada) subduction zone: Implications for the distribution of fluids. *Geology* 34, 53–56.
- Stanley, W., Boehl, J., Bostick, F., Smith, H., 1977. Geothermal significance of magnetotelluric sounding in the eastern Snake River Plain–Yellowstone region. *J. Geophys. Res.* 82, 2501–2514.
- Stanley, W.D., Mooney, W.D., Fuis, G.S., 1990. Deep crustal structure of the Cascade Range and surrounding regions from seismic refraction and magnetotelluric data. *J. Geophys. Res.* 95, 19419–19438.
- Stanley, W.D., Johnson, S.Y., Qamar, A.I., Weaver, C.S., Williams, J.M., 1996. Tectonics and seismicity of the southern Washington Cascade Range. *Bull. Seismol. Soc. Am.* 86 (1A), 1–18.
- Thomas, M., Sharpton, V., Grieve, R., 1987. Gravity patterns and Precambrian structure in the North American central plains. *Geology* 15, 489–492.
- Tian, Y., Zhao, D., 2012. Seismic anisotropy and heterogeneity in the Alaska subduction zone. *Geophys. J. Int.*
- Tian, Y., Sigloch, K., Nolet, G., 2009. Multiple-frequency SH-wave tomography of the western US upper mantle. *Geophys. J. Int.* 178, 1384–1402.
- Till, C.B., Grove, T.L., Carlson, R.W., Donnelly-Nolan, J.M., Fouch, M.J., Wagner, L.S., Hart, W.K., 2013. Depths and temperatures of 10.5 Ma mantle melting and the lithosphere–asthenosphere boundary below southern Oregon and northern California. *Geochem. Geophys. Geosyst.* 14, 1–16.
- Turcotte, D.L., Schubert, G., 2002. *Geodynamics*. Cambridge University Press.
- Türkoğlu, E., Unsworth, M., Pana, D., 2009. Deep electrical structure of northern Alberta (Canada): Implications for the diamond exploration. *Can. J. Earth Sci.* 46, 139–154.
- Vozoff, K., 1991. The magnetotelluric method. In: Nabighian, M.N. (Ed.), *Electromagnetic Methods in Applied Geophysics*, vol. 2B. Society of Exploration Geophysicists, Tulsa, OK, pp. 641–711.
- Wagner, L., Forsyth, D.W., Fouch, M.J., James, D.E., 2010. Detailed three-dimensional shear wave velocity structure of the northwestern United States from Rayleigh wave tomography. *Earth Planet. Sci. Lett.* 299, 273–284.
- Wang, D., Mookherjee, M., Xu, Y., Karato, S., 2006. The effect of water on the electrical conductivity of olivine. *Nature* 443, 977–980.
- Wannamaker, P.E., 2005. Anisotropy versus heterogeneity in continental solid earth electromagnetic studies: fundamental response characteristics and implications for physicochemical state. *Surv. Geophys.* 26, 733–765.
- Wannamaker, P.E., Booker, J.R., Jones, A.G., Chave, A.D., Filloux, J.H., Waff, H.S., Law, L.K., 1989. Resistivity cross section through the Juan de Fuca subduction system and its tectonic implications. *J. Geophys. Res.* 94, 14127–14144.
- Wannamaker, P.E., Doerner, W.M., Stodt, J.A., Johnston, J.M., 1997a. Subdued state of tectonism of the Great Basin interior relative to its eastern margin based on deep resistivity structure. *Earth Planet. Sci. Lett.* 150, 41–53.
- Wannamaker, P.E., Johnston, J.M., Stodt, J.A., Booker, J.R., 1997b. Anatomy of the southern Cordilleran hingeline, Utah and Nevada, from deep electrical resistivity profiling. *Geophysics* 62, 1069–1086.
- Wannamaker, P.E., Hasterok, D.P., Johnston, J.M., Stodt, J.A., Hall, D.B., Sodergren, T.L., Pellerin, L., Maris, V., Doerner, W.M., Groenewold, K.A., Unsworth, M.J., 2008. Lithospheric dismemberment and magmatic processes of the Great Basin–Colorado Plateau transition, Utah, implied from magnetotellurics. *Geochem. Geophys. Geosyst.* 9, Q05019.
- Wells, R.E., Engebretson, D.C., Snively, P.D., Coe, R.S., 1984. Cenozoic plate motions and the volcano–tectonic evolution of western Oregon and Washington. *Tectonics* 3, 275–294.
- Wells, E., McCaffrey, R., 2013. Steady rotation of the Cascade arc. *Geology* 41, 1027–1030.
- West, J.D., Fouch, M.J., Roth, J.B., Elkins-Tanton, L.T., 2009. Vertical mantle flow associated with a lithospheric drip beneath the Great Basin. *Nat. Geosci.* 2, 439–444.
- Whitmeyer, S.J., Karlstrom, K.E., 2007. Tectonic model for the Proterozoic growth of North America. *Geosphere* 3, 220–259.
- Worzewski, T., Jegen, M., Kopp, H., Brasse, H., Castillo, W.T., 2010. Magnetotelluric image of the fluid cycle in the Costa Rican subduction zone. *Nat. Geosci.* 4, 108–111.
- Wright, J.E., Wyld, S.J., 2006. Gondwanan, Iapetan, Cordilleran interactions: A geodynamic model for the Paleozoic tectonic evolution of the North American Cordillera. *Paleogeography of the North American Cordillera: Evidence for and against large-scale displacements*. *Spec. Pap., Geol. Assoc. Can.* 46, 377–408.
- Xue, M., Allen, R.M., 2010. Mantle structure beneath the western United States and its implications for convection processes. *J. Geophys. Res.* 115, B07303.
- Yoshino, T., 2010. Laboratory electrical conductivity measurement of mantle minerals. *Surv. Geophys.* 31, 163–206.
- Yoshino, T., Matsuzaki, T., Yamashita, S., Katsura, T., 2006. Hydrous olivine unable to account for conductivity anomaly at the top of the asthenosphere. *Nature* 443, 973–976.
- Yoshino, T., Laumonier, M., McIsaac, E., Katsura, T., 2010. Electrical conductivity of basaltic and carbonatite melt-bearing peridotites at high pressures: implications for melt distribution and melt fraction in the upper mantle. *Earth Planet. Sci. Lett.* 295, 593–602.
- Zhdanov, M.S., Smith, R.B., Gribenko, A., Cuma, M., Green, M., 2011. Three-dimensional inversion of large-scale EarthScope magnetotelluric data based on the integral equation method: Geoelectrical imaging of the Yellowstone conductive mantle plume. *Geophys. Res. Lett.* 38, L08307.
- Zhdanov, M., Gribenko, A., Cuma, M., Green, M., 2012. Geoelectrical structure of the lithosphere and asthenosphere beneath the northwestern United States. *J. Geol. Geosci.* 1, 2.
- Zimmerman, M.E., Zhang, S., Kohlstedt, D.L., Karato, S., 1999. Melt distribution in mantle rocks deformed in shear. *Geophys. Res. Lett.* 26, 1505–1508.